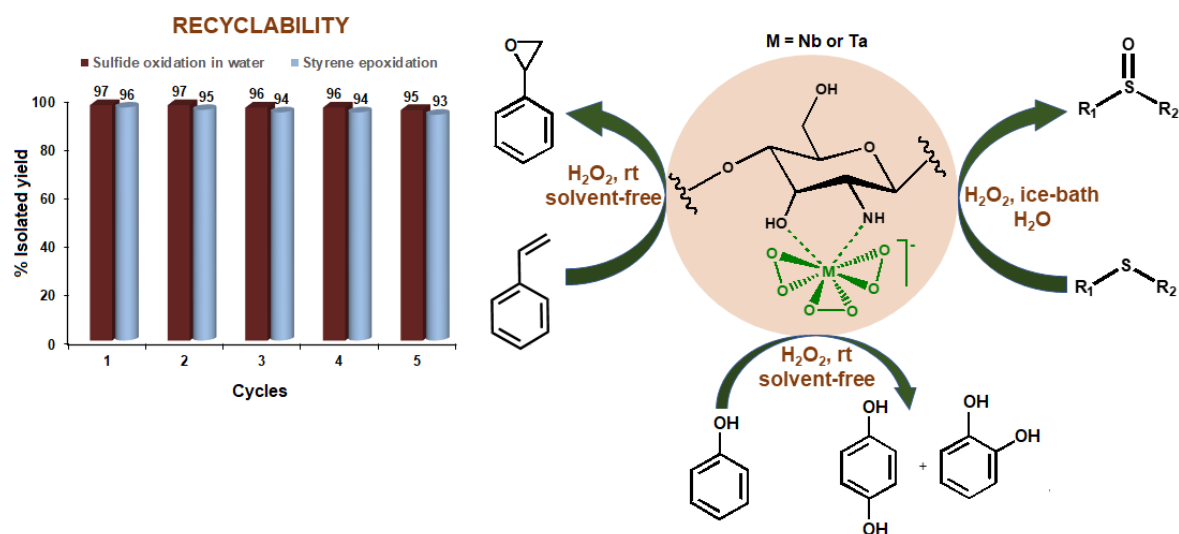# CHAPTER 5

Chitosan Supported Niobium(V) and Tantalum(V) Peroxido Complexes: Versatile Heterogeneous Catalysts for Eco-Compatible Organic Oxidations with H_2O_2 under Organic-Solvent-Free Conditions

5.1 Introduction

The importance of biopolymers such as chitin and chitosan as potential green support materials for the immobilization and heterogenization of metal catalysts [1-5] has been adequately delineated in Chapter 1. With numerous application possibilities in diverse areas ranging from biomedicines, wastewater treatment, fibre, cosmetic and food industries [2,4,6-10], chitosan and its derivatives have been recognized as immensely useful renewable substances with highly attractive physical and mechanical properties [2,6-7,11]. Due to a high content of hydroxyl and primary amino groups in the structure, chitosan is susceptible to facile functionalization and possesses an inherent ability to bind with various metal ions [2,7,8,11,12]. The advancement in the utilization of chitosan-based metal catalysts in a diverse range of organic transformations has been reviewed recently by Molnár [2]. There have been several reports describing the oxidation of various substrates such as cyclohexane, ethyl benzene, alcohol, toluene etc., over chitosan-supported metalloporphyrin as well as Schiff base complexes of transition metals, *viz.*, Mn, Fe, Cu, Co, Ni [2]. We have, however, noticed that the catalytic performance of well-defined pre-formed peroxidometal complexes immobilized on chitosan in organic oxidation has rarely been investigated [12,13]. Moreover, no data seems to be available pertaining to the catalytic application of chitosan-supported Nb and Ta based materials in organic transformations.

In the present study therefore, we considered it worthwhile to direct our efforts towards developing simple, sustainable and recyclable heterogeneous catalysts based on peroxido derivatives of Nb and Ta immobilized on chitosan and explore their efficiency in various organic oxidations. Selective oxidative transformations of organic substrates such as hydroxylation of phenol (PH) into hydroquinone (HQ) and catechol (CT), epoxidation of olefins, as well as oxidation of thioethers into sulfoxide/sulfone, represent some of the most essential and industrially important processes in organic synthesis [14-18]. The resulting oxygenated products, *viz*, epoxy compounds, sulfoxides/sulfone, as well as CT and HQ serve as key intermediates or precursors to a vast range of bio-active molecules [16-19], fine and commodity chemicals [14,15,20]. In addition, phenol being toxic, carcinogenic, and less biodegradable industrial waste [21,22], from the environmental standpoint, there has been tremendous emphasis on the transformation of phenol to value-added products. The phenomenal progress witnessed during the past decades in the field of catalytic organic oxidations resulted in the emergence of a plethora

of effective and high performing transition metal-based catalyst systems for accomplishing the aforementioned types of organic oxidations [14,23-31]. Nevertheless, methods which can satisfy all the requirements suitable for industrial goals (e.g., high productivity and selectivity along with cost efficiency and environmental acceptability) remain mostly elusive [14,25,27,28,31]. Thus, the uninterrupted quest for selective, sustainable and energy-efficient oxidation strategies which are compatible with benign solvent and green reagents, still continues [26,31,32].

In this respect, Nb and Ta-based catalysts are likely to be advantageous, as such systems have been reported to demonstrate better catalytic performance in organic oxidations with H_2O_2 as the oxidizing agent [33-38]. In fact, as Nb and Ta are known to be non-toxic and bio-inert, catalytic materials based on these metals are often considered particularly suitable for "green chemistry" applications [39,40]. Notwithstanding the important features like hydrolytic stability and ability to retain their activity in polar solvents as well as at high temperatures [33,34,41,42], the majority of heterogeneous Nb and Ta-based catalysts supported on porous SiO_2 or other metal oxides [36,37,43-52] were reported to show moderate activity in olefin epoxidations with H_2O_2 as oxidant. Similarly, microporous and mesoporous Nb-based catalysts in the H_2O_2 assisted hydroxylation of phenol often showed low productivity but high dihydroxybenzene selectivity [53-56]. On the other hand, so far, no report appears to exist on phenol hydroxylation catalyzed by a Ta-based system. Thus, to develop more productive catalyst systems to support organic oxidations under mild conditions still remains an important goal as well as a notable challenge in designing Nb and Ta-based solid catalysts.

In this Chapter, we report the preparation and characterization of a new chitosan supported catalyst $[Nb(O_2)_3(NH_2)(OH)]^-$–chitosan (**ChpNb**) (**5.1**). A chitosan anchored peroxidotantalum compound $[Ta(O_2)_3(NH_2)(OH)]^-$–chitosan (**ChpTa**), was synthesized previously in our laboratory [57]. An account of our findings on effectiveness of these supported pNb and pTa catalysts in the oxidation of three distinct types of organic substrates, *viz.*, phenol, styrene and sulfides using aqueous H_2O_2 as oxidant under mild and organic-solvent-free condition are presented herein.

5.2 Experimental section

5.2.1 Synthesis of Na[Nb(O₂)₃(NH₂)(OH)]–chitosan (ChpNb) (5.1)

The method involved the addition of 0.35 g of chitosan to a clear solution of the precursor complex, $Na_3[Nb(O_2)_4] \cdot 13H_2O$ (1.25 mmol, 0.65 g) with 30% H_2O_2 (4 mL), keeping the temperature below 4 ℃. The pH of the mixture was adjusted to 7 by adding a few drops of dilute HNO_3 (2 N, 0.65 mL). The reaction mixture was kept under the ice-cold condition, with occasional stirring for 24 hours. Then, the supernatant liquid was removed by decantation, and the residue was repeatedly treated with acetone and dried in vacuum.

5.2.2 Phenol hydroxylation

A typical reaction protocol was as follows: phenol (5 mmol, 0.47 g) and the catalyst (0.1 mmol of Nb or Ta) were placed in a 50 mL of round-bottomed flask (RB). To this mixture, 30% H_2O_2 (20 mmol, 2.26 mL) was added dropwise with continuous stirring. The reaction was carried out at room temperature, maintaining a metal: phenol: H_2O_2 molar ratio of 1:50:200. The products and the unreacted substrate were analyzed by high-performance liquid chromatography (HPLC).

The quantitative analysis of phenol and the oxidized products was done by a Thermo-Scientific Dionex Ultimate 3000 HPLC system equipped with a UV detector and a reversed-phase C18 column (250 × 4.6 mm). The maximum detection wavelength was 272 and the composition of the mobile phase was in a volume ratio of methanol: water = 3:7. Run time was 17 min with a 20 μL of injection volume and 1 mL/min of flow rate. The identification of the substrate and products was made by comparing the retention times with the respective authentic samples. A calibration curve was created with the authentic samples of phenol and the products using a range of concentrations (20-100 ppm). Then the content of the reaction mixture was determined by the interpolation of the calibration curve. The conversion of phenol (PH), yield of products and the selectivity of hydroquinone (HQ) and catechol (CT) were calculated by using the following equations:

$$\text{Conversion of phenol } (X_{\text{PH}}) = \frac{[\text{PH}]_i - [\text{PH}]_f}{[\text{PH}]_i} \times 100\% \quad (\mathbf{5.1})$$

$$\text{Yield of products } (Y_{\text{HQ+CT}}) = \frac{[\text{HQ}] + [\text{CT}]}{[\text{PH}]_i} \times 100\% \quad (\mathbf{5.2})$$

$$\text{Selectivity of HQ } (S_{\text{HQ}}) = \frac{[\text{HQ}]}{[\text{HQ}] + [\text{CT}]} \times 100\% \quad (\textbf{5.3})$$

$$\text{Selectivity of CT } (S_{\text{CT}}) = \frac{[\text{CT}]}{[\text{HQ}] + [\text{CT}]} \times 100\% \quad (\textbf{5.4})$$

where [PH], [HQ] and [CT] represent concentration of phenol, hydroquinone and catechol, respectively. i and f signify initial and final, respectively.

5.2.3 Styrene epoxidation

The reaction was initiated by the addition of 30% H_2O_2 (20 mmol, 2.26 mL) to a stirred mixture of styrene (5 mmol) and the catalyst (0.05 mmol of Nb or Ta) under magnetic stirring. The reaction occurred at room temperature, with a molar ratio of metal: styrene: H_2O_2 at 1:100:400. After completion, the products were extracted with ethyl acetate to analyze in HPLC.

Styrene and the respective oxidation products were quantitatively analyzed by HPLC utilizing the method described in **Section 3.2.4**, Chapter 3.

5.2.4 Oxidation of thioanisole (MPS)

The oxidation procedure was as follows: to a stirred mixture of MPS (5.0 mmol), catalyst (0.005 mmol of Nb or Ta) and 5 mL of H_2O in a 50 mL RB, 30% H_2O_2 (15 mmol, 1.7 mL) was added. The reactions were carried out at ice-bath condition (at <4 ℃), maintaining a metal: MPS ratio of 1:1000 and MPS: H_2O_2 ratio at 1:3. Thin-layer chromatography (TLC) was employed to monitor the reaction progress. After completion of the reaction, the products were analyzed by the method described in **Section 3.2.5** of Chapter 3 (**Appendix IV**).

5.2.5 Procedure for control experiments

The control experiments were carried out separately for phenol hydroxylation, styrene epoxidation, and sulfide oxidation in the absence of the catalyst. For phenol hydroxylation as well as styrene epoxidation, the control reaction was conducted at room temperature under solventless condition with 5 mmol of substrate (phenol or styrene) and 20 mmol of 30% H_2O_2 and the reaction progress was monitored over 5 and 8 h for phenol hydroxylation and styrene epoxidation, respectively. The blank reaction for sulfide oxidation was initiated by the addition of 30% H_2O_2 (15 mmol) to a stirred mixture of

MPS (5 mmol) and water (5 mL) at ice-bath temperature.

5.2.6 Catalyst regeneration

The catalyst, **ChpNb** (**5.1**) was easily separable from the reaction mixture and applied for up to five successive cycles. The recyclability experiment of the catalyst was conducted individually using styrene and MPS as substrates. After completion of the first reaction cycle of styrene epoxidation under the optimized condition, the catalyst was separated from the spent reaction mixture by simple filtration or centrifugation, then washed repeatedly with acetone and dried *in vacuo*. Subsequently, a new cycle of reaction was performed with the recovered catalyst using a fresh batch of styrene and 30% H_2O_2 under solvent-free condition maintaining a metal: styrene molar ratio of 1:100 and styrene: H_2O_2 ratio of 1:4. In case of the sulfoxidation reaction, after completion of the reaction, the catalyst was separated and repeatedly washed with acetone and dried. The recovered catalyst was applied for the next cycle of reaction with a new batch of the MPS maintaining the metal: MPS and MPS: H_2O_2 molar ratios of 1:1000 and 1:3, respectively. The content of the reaction mixture for styrene was analyzed by HPLC, and in the case of MPS oxidation, TLC was employed to study the progress of the reaction.

5.3 Results and discussion

5.3.1 Synthesis

The synthetic route developed for obtaining chitosan-supported solid complex **ChpNb** (**5.1**) involves a fairly simple methodology based on the reaction of chitosan with the tetraperoxidometallate precursor complex, $Na_3[Nb(O_2)_4]\cdot13H_2O$ (**TpNb**) in the presence of 30% H_2O_2 in water, at ice-bath temperature. Chitosan being water soluble under acidic conditions [58-60], the maintenance of the reaction pH >7 was found to be crucial for obtaining the solid catalysts in water-insoluble form. Importantly, the compound is non-hygroscopic in nature and remain stable and catalytically active for weeks. This feature of the complex is indeed noteworthy, considering that peroxidometallates generally tend to be hygroscopic in nature [58].

5.3.2 Characterization

Various spectroscopic and analytical techniques, namely elemental analysis, SEM-EDX, powder XRD, XPS, BET, TG-DTG, FT-IR, Raman and ^{13}C NMR analysis, were

employed to characterize the synthesized complex. The Metal: O_2^{2-} ratio (1:3) obtained from the ICP-OES and elemental analysis results (**Table 5.1**) testified to the presence of three peroxido groups attached to each Nb center in the compound. The metal loading on chitosan support was found to be 0.70 mmol/g of the polymer for the complex. The magnetic susceptibility measurements and XPS analysis further indicated the diamagnetic nature of the peroxidoniobium complex as well as the existence of the Nb in a +5 oxidation state.

Table 5.1: Analytical data for the synthesized complex **ChpNb (5.1)**

Complex	% Found from elemental analysis (% obtained from EDX spectra)					O_2^{2-}	Nb: O_2^{2-}	Nb loading[a] (mmol g^{-1} of polymer)
	C	H	N	Na	Nb			
ChpNb	42..02	4.85	5.45	-	6.44[b]	6.86	1:3	0.7
	(41.93)	-	(5.57)	(1.24)	(6.52)	-		-

[a]Metal loading $= \dfrac{\text{Observed metal \% X 10}}{\text{Atomic weight of metal}}$

[b]Determined by ICP-OES analysis

5.3.2.1 SEM and EDX analysis

Field emission scanning electron microscopy (FESEM) was employed to study the surface topography of pure chitosan as well as the polymer immobilized complex and the corresponding FESEM images with different sizes are presented in **Fig. 5.1**. In addition, the SEM images of the pure polymer and those of the chitosan anchored pNb complex are included in **Fig. 5.2**. Both FESEM and SEM images displayed distinct morphological changes occurring after metal incorporation. Such observation clearly suggested the chemical modification of chitosan due to adsorption or dispersion of the peroxidoniobium species on the chitosan surface.

The EDX analysis data, which provides *in situ* chemical analysis of the bulk, furnished further evidence for the presence of Nb as the component of the complex in addition to O, N, C, and Na atoms [**Fig. 5.2 (e)**]. The EDX analysis was carried out by focusing on multiple regions of the compound surface, and the composition obtained from EDX results concurred well with the elemental analysis values.
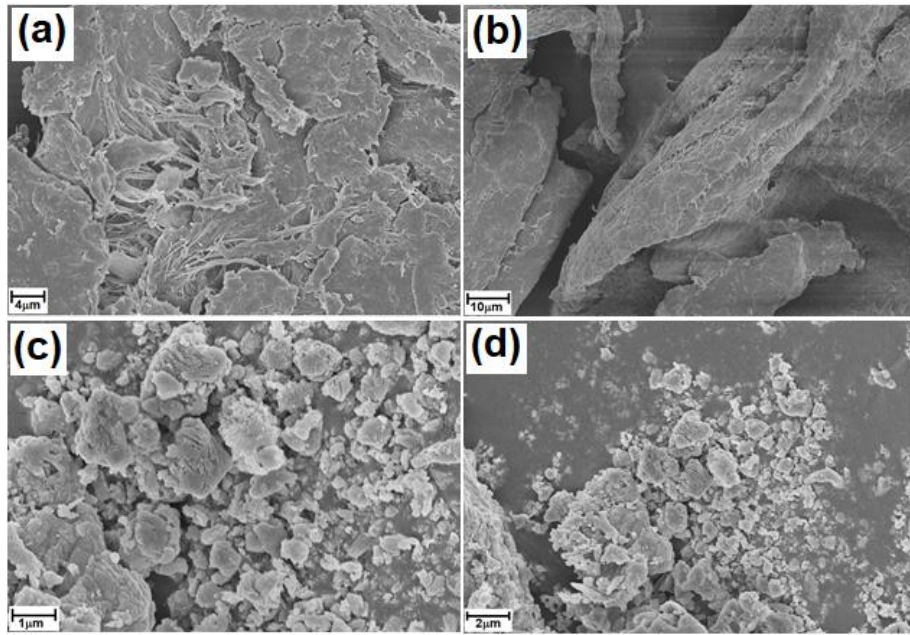
Fig. 5.1 FESEM images of **Chitosan** (a) 4 μm, (b) 10 μm; **ChpNb** (c) 1 μm, (d) 2 μm.
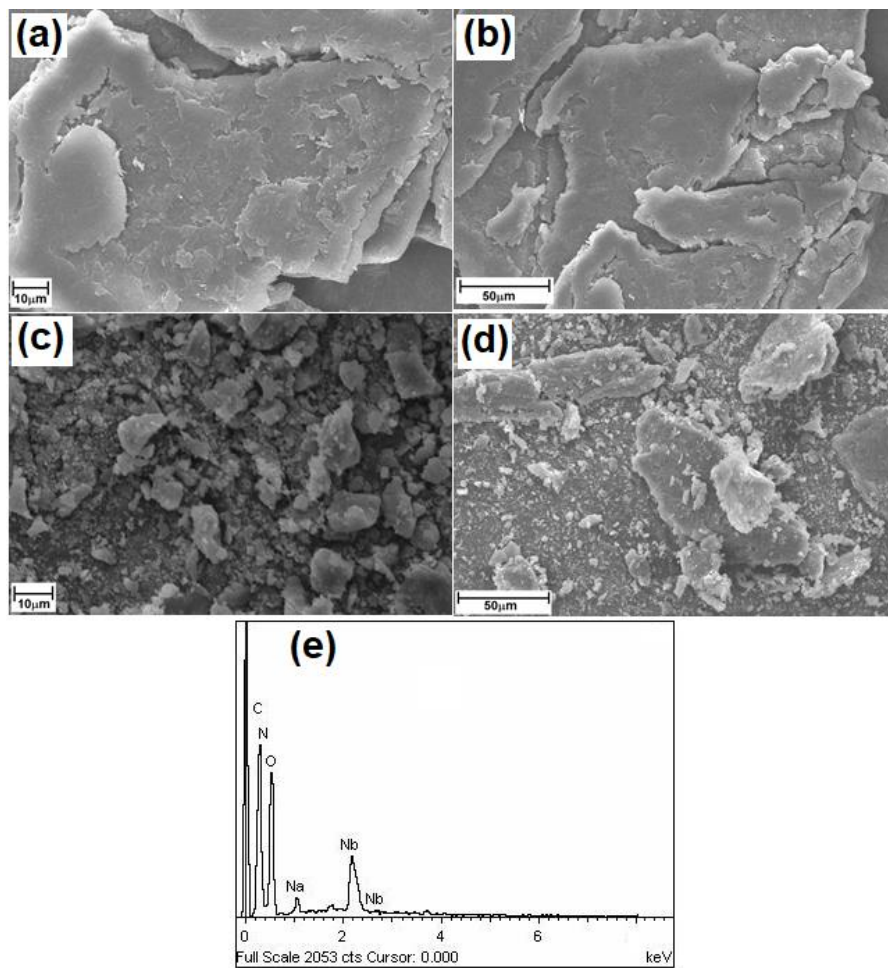
Fig. 5.2 SEM images of **Chitosan** (a) 10 μm, (b) 50 μm; **ChpNb** (c) 10 μm, (d) 50 μm and (e) EDX spectrum of **ChpNb**.

**5.3.2.2 Powder X-ray diffraction analysis**

The powder XRD patterns of pure chitosan and metal anchored polymeric complex **5.1**, are depicted in **Fig. 5.3**. Pure chitosan showed three distinct diffractions at 2θ values of *ca.* 12.7, 19.9 and 26.7°, respectively, corresponding to the semi-crystalline nature of the polymer [61-63]. After the anchoring of the pNb species to the polymer, the intensities of these characteristic peaks visibly weakened, probably due to the disruption of H-bonds within the chitosan matrix caused by metal complexation [62,64]. A number of new sharp peaks appeared in the diffractogram of the catalyst at 2θ values of *ca.* 18.0, 19.8, 21.0, 29.6 and 30.6° indicating the formation of a new crystalline phase. These additional peaks are attributed to the (111), (020), (200), (022) and (202) planes for **ChpNb** (**5.1**) (PDF 52-0708). Thus, the PXRD results further confirmed the successful immobilization of the peroxidometal moiety on the biopolymer support.
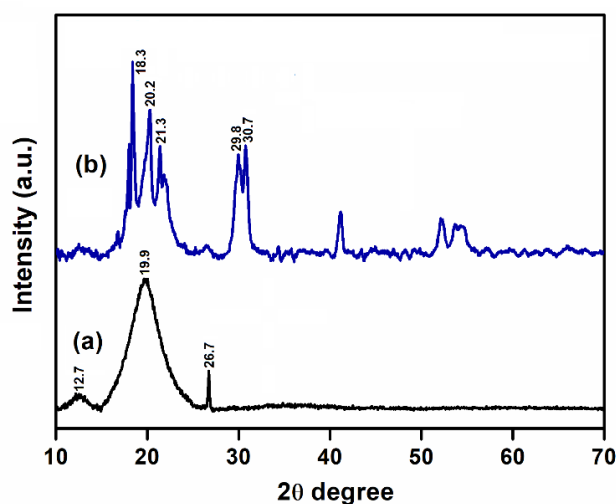
Fig. 5.3 PXRD patterns of (a) **Chitosan** and (b) **ChpNb** (**5.1**).

**5.3.2.3 X-ray photoelectron spectroscopy**

The XPS and survey spectra of **ChpNb** (**5.1**) are shown in **Fig. 5.4**. The XPS spectrum of the complex **5.1** [**Fig. 5.4** (a)] exhibited two well-resolved peaks located at binding energies (BE) of 207.1 and 209.8 eV, corresponding to the components of $3d_{5/2}$ and $3d_{3/2}$ doublet of Nb in +5 oxidation state [65,66]. The successful anchoring of Nb(V) to chitosan has been further proved by peaks appearing at BE values characteristic of oxygen, nitrogen and carbon [**Fig. 5.4** (b)].
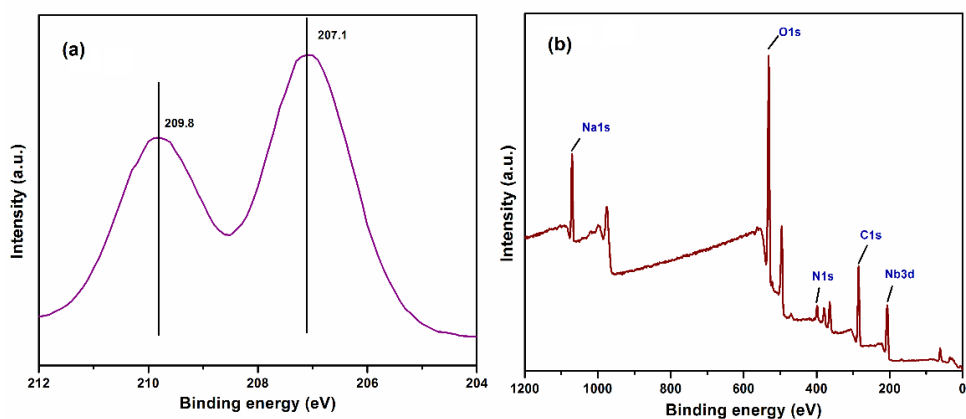
Fig. 5.4 (a) XPS spectrum and (b) XPS survey spectrum of **ChpNb** (**5.1**).

5.3.2.4 BET analysis

The specific surface area of the metal incorporated chitosan complex and the untreated polymer was measured by utilizing BET analysis with the nitrogen adsorption method [67], and pore volume was obtained by the BJH model [68]. The compound showed characteristic type II N_2 adsorption/desorption isotherm (**Fig. 5.5**) of an IUPAC standard on particles which have macropores and nonpores [69,70]. The data listed in **Table 5.2** clearly show the distinct changes occurring in the surface morphology of the biopolymer after complexation with the metal. The average specific surface area was found to be 13.1 for **ChpNb**, which is considerably higher than that of the neat chitosan (4.6 m^2/g) (**Table 5.2**). For the complex, the constant C of the BET equation was in the 2-200 range explaining multilayer adsorptions (type II isotherm) [71].
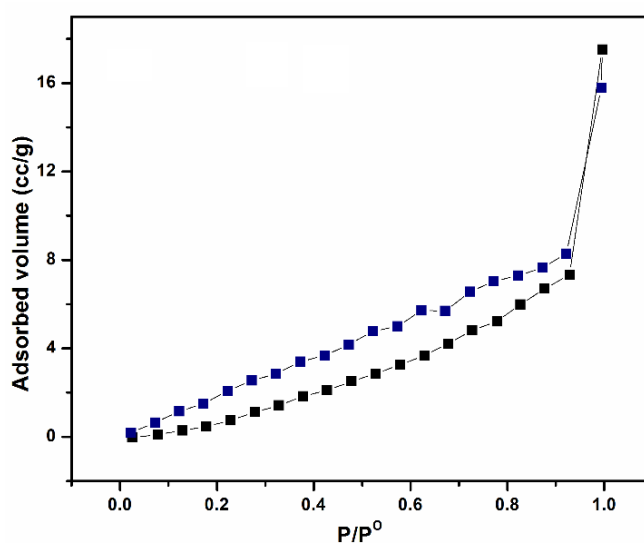
Fig. 5.5 Adsorption/desorption isotherm of **ChpNb** (**5.1**).

Table 5.2: BET surface area, V_{tot} and the pore radius of chitosan and polymer bound peroxidometal complex

| Compound	$S_{BET}^a (m^2/g)$	$V_{tot}^b (mL/g)$	Pore radius (Å)
Chitosan	4.6	0.01	17.1
ChpNb	13.1	0.03	20.2

[a]BET surface area. [b]Total pore volume.

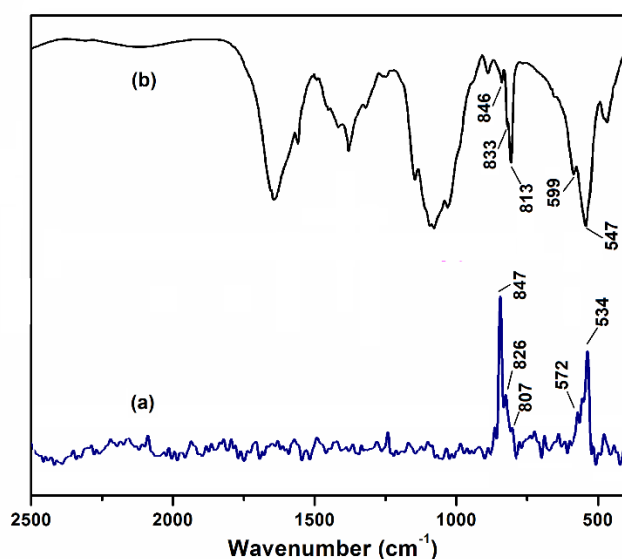### 5.3.2.5 FTIR and Raman spectral analysis

Information gathered from a comparative study of FTIR spectra (**Fig. 5.6**) as well as Raman spectral analysis (**Fig. 5.7**) of pure polymer and metal anchored complex **ChpNb** (**5.1**) allowed us to surmise that both the -NH₂ and -OH groups of chitosan participate in immobilization of peroxidometal complex. The IR spectra, as well as the complementary Raman spectra of the peroxidoniobium complex, showed three typical absorption peaks for ν(O-O) in the 800-900 cm⁻¹ range signifying the formation of triperoxidoniobium species [72-74]. The $\nu_{sym}(M-O_2)$ and $\nu_{asym}(M-O_2)$ vibrations of the complex were observed in the 500-600 cm⁻¹ region.

The free chitosan showed typical vibrations at *ca.* 1646 cm⁻¹ (C–O stretching and N-H deformation mode, amide I) [62,63,75] along with 1154 (bridging O stretch), 1592 (N-H bending), 2876 (-CH₂ stretching), 2921 cm⁻¹ (-CH₃ stretching) [63,76,77]. Involvement of the amide group in metal coordination could be negated from the nearly unaltered position of the amide I band in the spectrum of the complex in comparison to the unbound polymer. A considerable shifting in the stretching vibration of -NH₂ and -OH group (3434 cm⁻¹) to the lower frequency of 3419 cm⁻¹ in the complex **ChpNb** (**5.1**) suggested the participation of either of these groups in the complexation [6,8,76,77]. Furthermore, the considerable decrease in intensity of the band corresponding to -OH bending vibration at *ca.* 1421 cm⁻¹ in the complex indicated the likelihood of coordination through -OH group. Along with that, the shift in the vibrational frequency of the secondary -OH group (at 1089 cm⁻¹) to around 1080 cm⁻¹ in the spectra of the peroxidometallate suggested the involvement of the secondary -OH group in the metal coordination. The absorption due to the primary -OH group of the chitosan at *ca.* 1038 cm⁻¹ remained unaffected throughout the metal coordination. Along with this, the observed shifting in the -NH bending vibration of the amine group of chitosan from 1592 cm⁻¹ to the lower

wavenumber of *ca.* 1563 cm^{-1} in the complex indicated the bonding of the nitrogen center of the chitosan to the metal ion [6,8,76]. These evidences confirmed the coordination of the polymer with the metal *via* both the -NH$_2$ and -OH groups. The presence of the characteristic peaks of chitosan, β-(1–4) glycoside bridging bands (at *ca.* 894 and 1154 cm^{-1}) in the complex indicated the successful attachment of chitosan to the metal without affecting the backbone of the biopolymer [62,64,75].
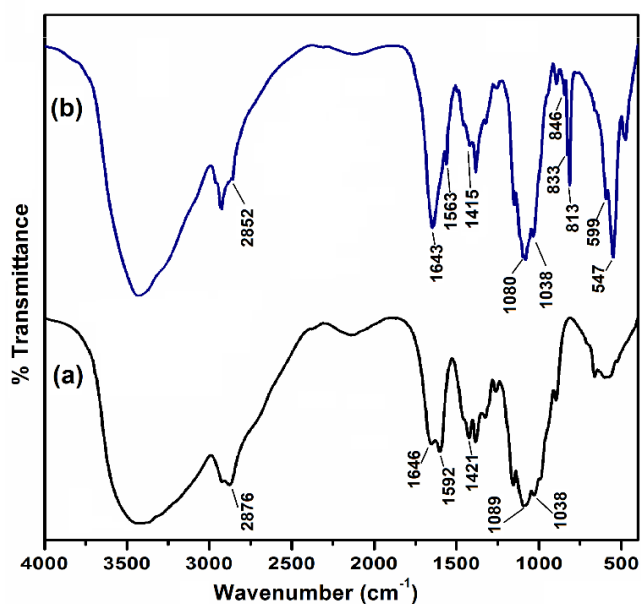

Fig. 5.6 FTIR spectra of (a) **Chitosan** and (b) **ChpNb** (**5.1**).

Fig. 5.7 (a) Raman spectrum of **ChpNb** (**5.1**) and (b) FTIR spectrum of **ChpNb** (**5.1**).

5.3.2.6 Electronic spectral analysis

The diffuse reflectance UV-visible spectrum of the compound **ChpNb** (**5.1**) showed two distinct bands within the range of 200-400 nm (**Fig. 5.8**). The absorption occurring within the 350-380 nm region could be assigned to the peroxido ligand to metal transition (LMCT) characteristic of peroxidometallate species of Nb(V) [78,79]. On the other hand, the band with a maximum at *ca.* 250 nm in the spectrum of the complex was attributed to the typical intra-ligand n→π* or π→π* transitions of the chitosan support [76,80].
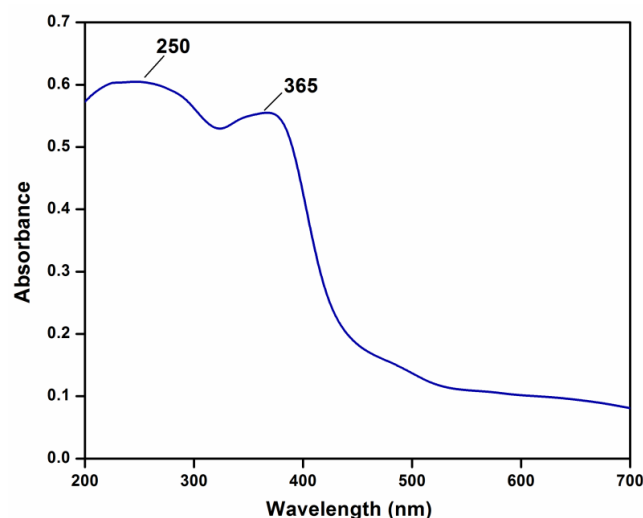

Fig. 5.8 Diffuse reflectance UV-visible spectrum of **ChpNb** (**5.1**).

5.3.2.7 ^{13}C NMR analysis

The solid-state ^{13}C NMR spectra of the polymer-supported compound **5.1** and the pure chitosan are presented in **Fig. 5.9**. The respective chemical shift values are listed in **Table 5.3**. Usually, the spectrum of the pristine chitosan displays resonances at *ca.* 105.9, 57.7, 83.1, 61.3, and 23.4 ppm corresponding to C-1, C-2, C-4, C-6, and CH$_3$ carbon atoms, respectively [81-83]. The signal at 76.2 ppm probably occurs due to a combination of C-3 and C-5 peaks [81-83]. After loading of the metal into the chitosan caused a distinct shift of the signals corresponding to C-2 and C-3 carbon atoms attached to -NH$_2$ and -OH groups, respectively by nearly 1 ppm, compared to the ^{13}C NMR spectrum of the original polymer. The observed shift may be attributed to the participation of these groups in metal binding [59,81,83]. Significantly, no new signal was observed at *ca.* 175 ppm in the spectrum corresponding to -COOH group and the overall spectral pattern of the compound

resembled closely the spectrum of free chitosan. Thus, the ^{13}C NMR results demonstrate that, despite the structural modification of chitosan as a consequence of complexation, the main backbone structure of the polymer remained unchanged during the immobilization of peroxidoniobium species [58,59,84].
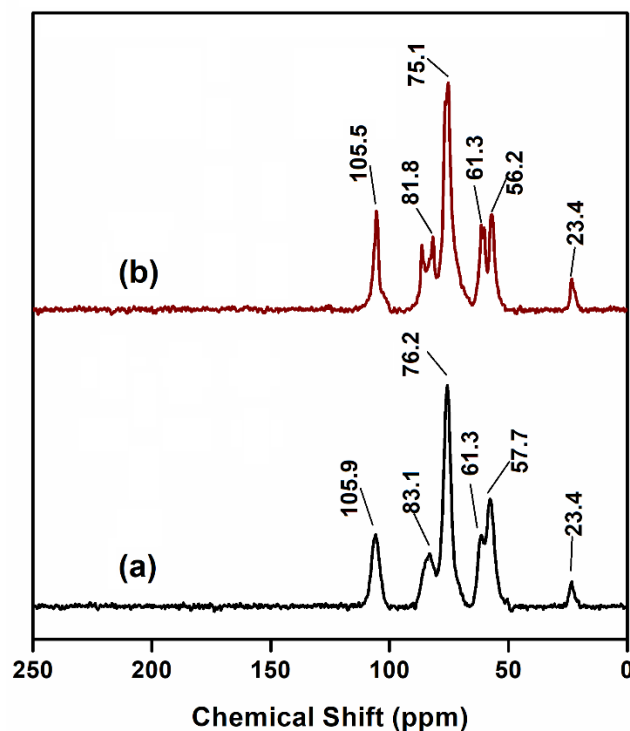
Fig. 5.9 ^{13}C NMR spectra of (a) **Chitosan** and (b) **ChpNb** (**5.1**).

Table 5.3: ^{13}C NMR spectral data for chitosan and chitosan anchored pNb complex

Compound	Chemical shift (ppm)					
	C-1	C-2	C-3–C-5	C-4	C-6	CH$_3$
Chitosan	105.88	57.65	76.15	83.11	61.32	23.37
ChpNb	105.51	56.22	75.09	81.76	61.32	23.37

See **Fig. 5.11** for atom numbering

5.3.2.8 Thermogravimetric analysis

Thermogram of the chitosan anchored pNb compound **5.1** showed multistep degradation on heating up to 700 ℃ (**Fig. 5.10**, **Table 5.4**) with the initial step of degradation occurring below 100 ℃ due to dehydration. This was followed by the

degradation in the temperature range of 133-207 ºC with a mass loss of 6.8 % resulting in the removal of peroxido groups from the peroxidometallate species. The complex undergoes further degradation resulting from the rupture of the glycosidic linkage of the chitosan backbone in the 206-631 ºC range [62,85]. After complete degradation of the complex, the % of residue remaining was found to be 35.2%. The IR spectra of the residue was devoid of chitosan bands and displayed the typical ν(Nb=O) bands of oxidoniobium species.
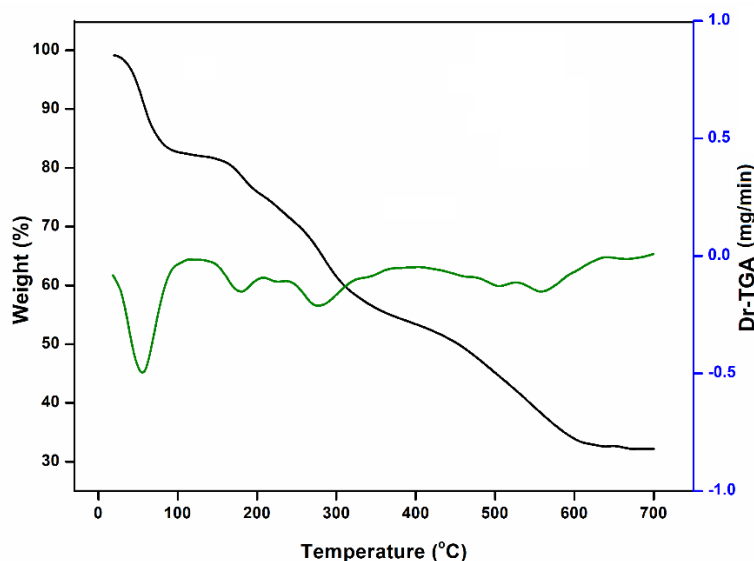

Fig. 5.10 TGA-DTG plots of **ChpNb** (**5.1**).

Table 5.4: Thermogravimetric analysis data of the polymer immobilized complex

Compound	Temperature range (°C)	Observed weight loss (%)	Final residue (%)
ChpNb	31-98	15.5	35.2
	133-207	6.8	
	211-631	42.5	

In the light of the above collective evidences, the type of structure proposed for the chitosan anchored complex **ChpNb** (**5.1**) is shown schematically in **Fig. 5.11**. In order to describe the mode of metal-chitosan coordination, various models such as the 'bridge model' and 'pendant model' have been suggested previously [6,8,86]. The pendant model depicts the coordination of metallic ion *via* the amino group of chitosan as a pendant [6,86]. Whereas, in the bridged model, bonding of the metal ion occurs through four N atoms of

the same or different chains of the polymer [6,86]. In the proposed structure for the compound, coordination of the Nb(V) to the amino group of the polymer appears to form a 'pendant'-type structure with an additional bond of Nb-OH, completing the eight-fold coordination around the metal center.
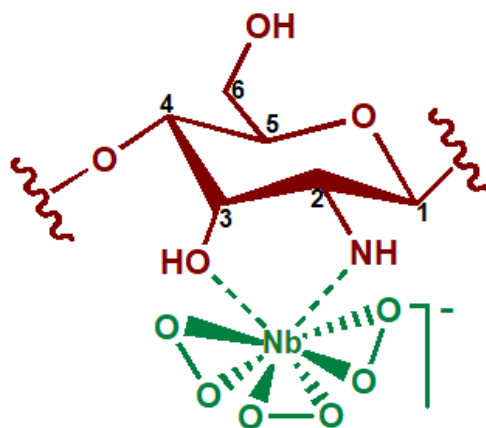
**Fig. 5.11** Proposed structure of **ChpNb** (**5.1**). " ∿∿∿ " represents polymer chain.

5.3.3 Catalytic activity

5.3.3.1 Phenol hydroxylation

The catalytic potential of the Nb as well as previously synthesized Ta [57] peroxido compounds immobilized on chitosan was first tested in the hydroxylation of phenol using 30% H_2O_2 as a terminal oxidant. To start with, a reaction was carried out with **ChpNb** (**5.1**) as the representative catalyst maintaining an Nb: phenol molar ratio of 1:250 and phenol: H_2O_2 ratio of 1:4, as shown in **Table 5.5**, entry 1 and **Fig. 5.12**. The reaction was conducted at room temperature, without the addition of any extra solvent. Under this reaction condition, as revealed by HPLC analysis, over 23% of phenol was converted to the desired dihydroxybenzene products, hydroquinone (HQ) and catechol (CT) within 5 h of reaction time. There was no evidence for the formation of any over-oxidized products such as *o*- or *p*-benzoquinone [HPLC chromatogram and GC-MS spectra (**Appendix V, Fig. IIIA** and **IVA**)]. The selectivity ratio of HQ/CT (2.5:1) demonstrated the preferential formation of *p*-product (HQ) over the *o*-product (CT) during the catalytic process. The preliminary experiment was followed by a survey of reaction parameters, *viz*., catalyst loading, oxidant concentration, reaction time, and solvent. Details of the optimization studies are compiled in **Table 5.5** and are also illustrated in **Fig. 5.12-5.16**.

Under the above reaction conditions, an increase in the catalyst loading from an Nb: phenol ratio of 1:250, keeping other reaction parameters constant, resulted in a steady increase in the conversion of phenol [**Fig. 5.12** and **Table 5.5** (entry 1-4)]. The catalyst displayed excellent dihydroxybenzene selectivity of 100% with a consistent HQ/CT ratio of ~2:1, irrespective of the catalyst concentration. Thus, the results showed the domination of p-hydroxy species (hydroquinone) as the favoured product. A maximum of 35% conversion was attained with an Nb: phenol ratio of 1:50 (**Table 5.5**, entry 4). Significantly, the highest TON value of 80 was achieved with a very low catalyst loading (Nb: phenol =1:500). Nevertheless, the Nb: phenol ratio of 1:50 was selected for further studies keeping in view the better phenol conversion obtained with this molar ratio. The improvement in phenol conversion with an increment in catalyst concentration could tentatively be explained by an increase in the availability of a number of catalytic active sites. It is worthy to note that, under these reaction conditions, phenol conversion and total yield of products (CT and HQ) were found to be 35.1 and 34.7%, respectively. From this small discrepancy observed between these two data (<0.5%) formation of additional undetectable by-products such as tar, during the process of phenol hydroxylation in the present case, appears to be negligible. This is a remarkable observation keeping in view that the major reaction products of phenol hydroxylation, CT and HQ are often known to be accompanied by the formation of some amount of benzoquinone and
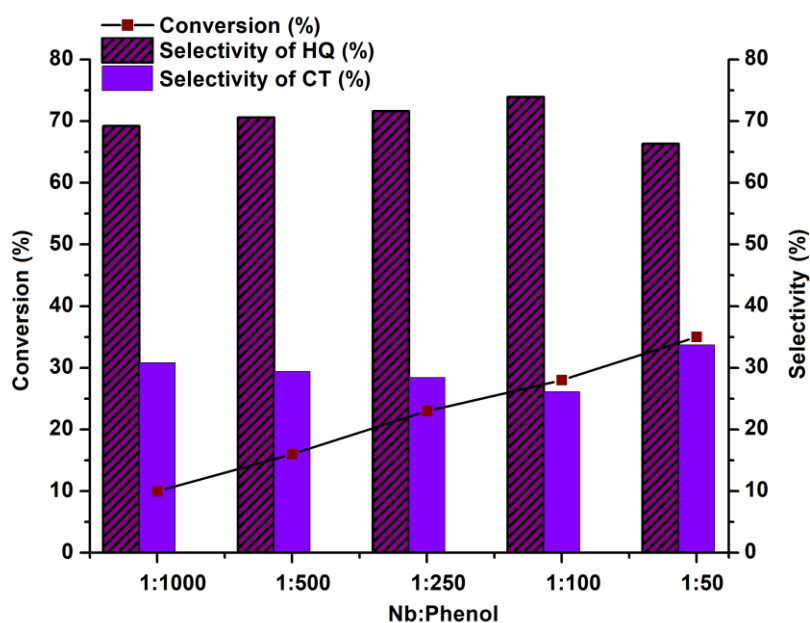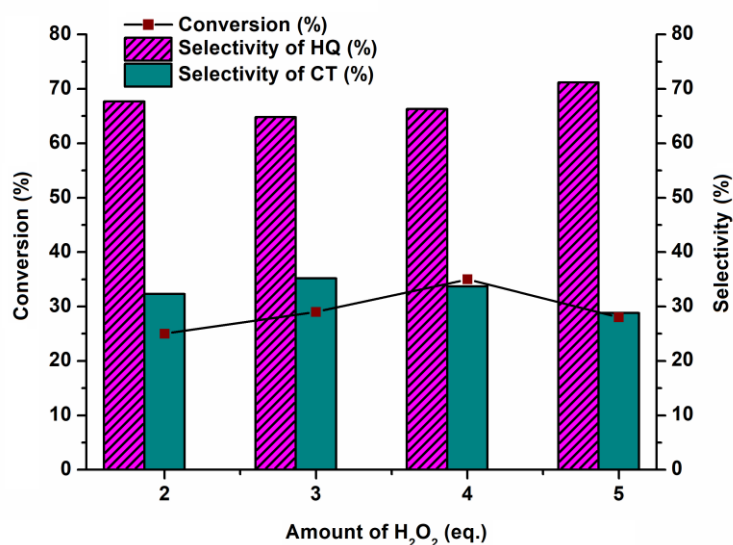

Fig. 5.12 Effect of catalyst loading on phenol hydroxylation. Reaction conditions: Phenol (5 mmol), 30% H_2O_2 (20 mmol), room temperature, 5 h, without solvent.

chromatographically undetectable tar as by-products [87-89]. That the catalyst plays an essential role in facilitating the hydroxylation process is evident from the negligible (~0.1%) conversion of phenol obtained from a blank reaction conducted without the catalyst under otherwise analogous reaction conditions [**Table 5.5** (entry 14)].

Similarly, a concentration dependent study was performed with respect to the phenol: H_2O_2 stoichiometry by varying the amount of H_2O_2 from 2-5 equivalents keeping other variables fixed as shown in **Fig. 5.13** and **Table 5.5** (entries 4-7). The reactions proceeded without any significant alteration in the CT/HQ selectivity and afforded the maximum phenol conversion at a Phenol: H_2O_2 molar ratio of 1:4. Importantly, further increment of oxidant amount to 5 equivalents reduced the overall conversion of phenol [**Fig. 5.13** and **Table 5.5** (entry 7)]. Such phenomenon is not unusual in the case of phenol hydroxylation, as revealed by previous reports and our own experience [17,90,91], which has been attributed to the dilution effect prevailing at higher concentration of liquid oxidant beyond the optimal requirement of the oxidant [17,90,91].

The impact of time on phenol conversion and product selectivity was studied over a time span of 6 h. A gradual increase in the conversion of phenol to the desired products (CT and HQ) was observed up to 5 h of reaction time [**Table 5.5** (entries 4, 8-12) and **Fig. 5.14**]. Extending the reaction time beyond 5 h, led to a slight decrease (*ca*. 2%) in phenol conversion. This may possibly occur due to the formation of a trace amount of

Fig. 5.13 Effect of H_2O_2 concentration on phenol hydroxylation. Reaction conditions: Phenol (5 mmol), catalyst (0.1 mmol of Nb), RT, t = 5 h, without solvent.

chromatographically undetectable tar, resulting from the further oxidation of hydroquinone and catechol. Such observation in case of phenol hydroxylation is not unprecedented [87-89]. Interestingly, the product selectivity remained almost unchanged throughout the duration of the reaction.
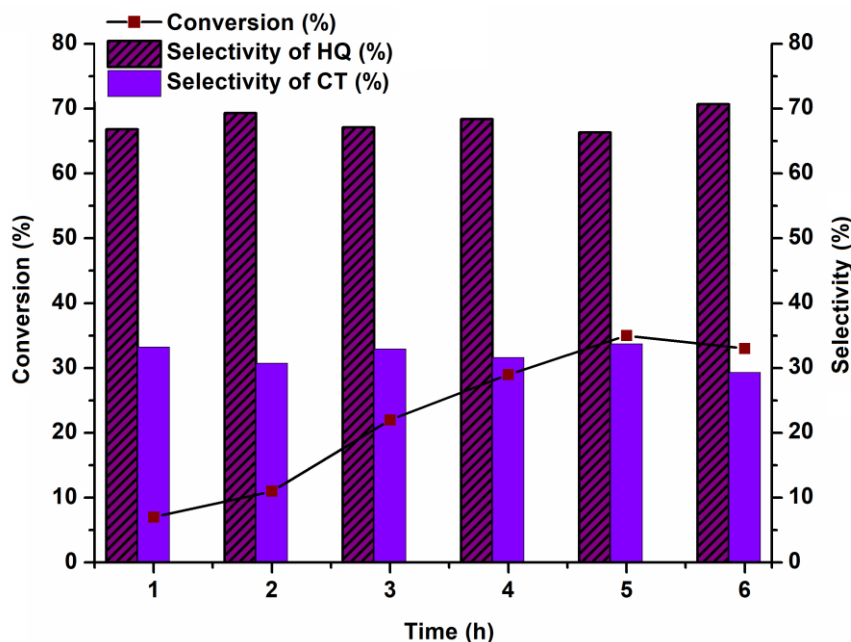
Fig. 5.14 Conversion of phenol with time. Reaction Conditions: 5 mmol of substrate, 30% H_2O_2 (20 mmol), catalyst (0.1 mmol of Nb), without solvent, RT.

Subsequently, we have examined the performance of the solid catalyst in presence of various polar and non-polar organic solvents as well as in water, as both the catalysts were insoluble in these solvents at room temperature. Interestingly, among the solvents screened, the catalyst was found to be most compatible with water, as revealed by the superior results obtained in an aqueous medium both in terms of dihydroxybenzene selectivity (HQ: CT selectivity ratio of nearly 3:1) as well as phenol conversion (**Fig. 5.15**). These findings further signified the water-tolerant nature of the catalyst. Good phenol conversion was also observed in other polar solvents, *viz*., methanol and ethanol, although the reaction was accompanied by the formation of benzoquinone as an additional minor by-product, causing a drop in product selectivity. Our observations are consistent with several previous studies, which showed that phenol conversion and biphenol selectivity generally improved with increasing solvent polarity [92-94]. The formation of benzoquinone along with dihydroxybenzene has often been a common phenomenon in phenol hydroxylation conducted in the organic solvent [55,92,93]. The catalysts however

provided maximum conversion under solvent-free condition. The greater efficiency of the catalyst system observed without additional solvent may be attributed to the higher reactant concentration in this case. Similar findings were reported in the case of many of the solvent-free procedures [95,96].

Table 5.5: Optimization of reaction conditions for selective hydroxylation of phenol catalyzed by **ChpNb** (**5.1**)[a]

Phenol (PH) → ChpNb, 30% H_2O_2, RT → Hydroquinone (HQ) + Catechol (CT)

| Entry	Molar ratio (Cat:PH)	30% H_2O_2 (eq.)	Time (h)	Conversion of phenol (%)	TON[b]	Selectivity (%) HQ	Selectivity (%) CT
1	1:250	4	5	23	58	71.6	28.4
2	1:500	4	5	16	80	70.6	29.4
3	1:100	4	5	28	28	73.9	26.1
4	**1:50**	**4**	**5**	**35**	**18**	**66.3**	**33.7**
5	1:50	2	5	25	13	67.7	32.3
6	1:50	3	5	29	15	64.8	35.2
7	1:50	5	5	28	14	71.2	28.8
8	1:50	4	1	7	4	66.8	33.2
9	1:50	4	2	11	6	69.3	30.7
10	1:50	4	3	22	11	67.1	32.9
11	1:50	4	4	29	15	68.4	31.6
12	1:50	4	6	33	17	70.7	29.3
13[c]	1:50	4	5	32	16	64.8	35.2
14[d]	-	4	5	0.1	-	72.1	27.9

[a]Reaction conditions: 5 mmol Phenol, room temperature. [b]TON (turn over number) = mmol of substrate consumed per mmol of Nb. [c]Scaled-up reaction with 4.7 g of substrate. [d]Blank reaction without any catalyst.
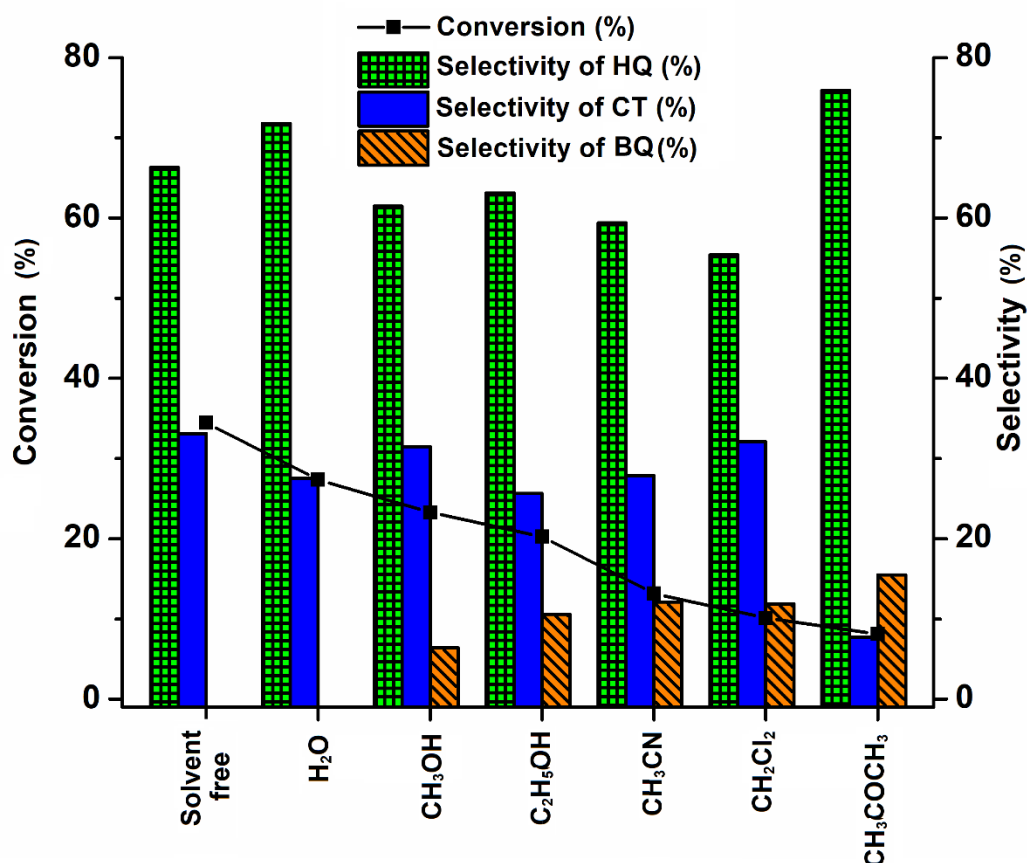
Fig. 5.15 Effect of solvent on phenol conversion. Reaction conditions: phenol (5 mmol), oxidant (20 mmol), catalyst (0.1 mmol of Nb), solvent (5 mL), RT, 5 h.

Having determined the optimum reaction conditions for phenol hydroxylation using the catalyst **ChpNb** (**5.1**), the efficiency of the chitosan-supported peroxidotantalum catalyst (**ChpTa**) [57] was tested under similar condition. **Fig. 5.16** reveals that the Nb-based catalyst **ChpNb** showed slightly superior activity *vis-à-vis* its tantalum-containing analog, although hydroquinone selectivity was observed to be relatively higher in the case of the catalyst **ChpTa.** On the other hand, significantly lower conversion of phenol with a slightly higher hydroquinone selectivity was obtained when the neat unsupported precursor complexes, $Na_3[Nb(O_2)_4]\cdot 13H_2O$ (**TpNb**) or $Na_3[Ta(O_2)_4]\cdot H_2O$ (**TpTa**) [57] were used in lieu of the supported catalysts (**Fig. 5.16**), maintaining the same Nb or Ta loading under the same optimized condition (RT, Nb: phenol = 1:50, phenol: H_2O_2 = 1:4 and t = 5 h). It is thus clear that immobilization of the peroxido species on the chitosan support plays an affirmative role in enhancing the catalytic performance of such species.
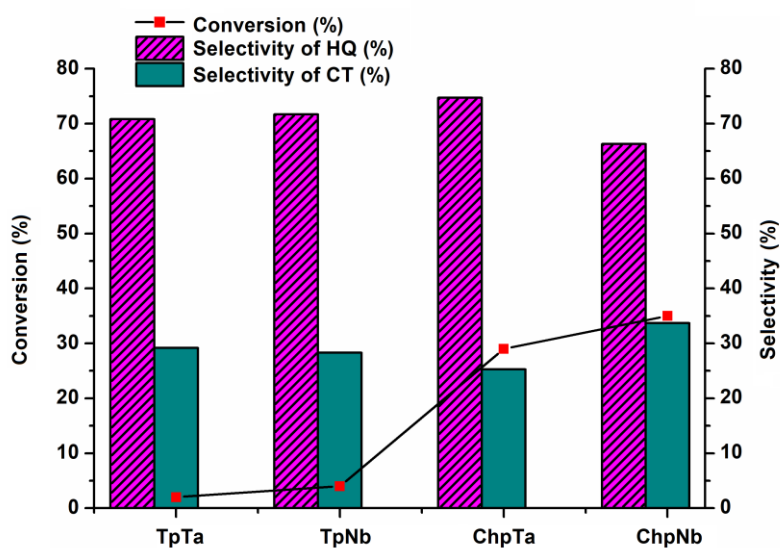
Fig. 5.16 Diagram showing the conversion of phenol and selectivity of HQ and CT by **ChpNb**, **ChpTa** along with the precursor complexes, $Na_3[Nb(O_2)_4]·13H_2O$ (**TpNb**) and $Na_3[Ta(O_2)_4]·H_2O$ (**TpTa**). [a]Reaction conditions: Phenol (5 mmol), catalyst (0.1 mmol of metal), H_2O_2 (20 mmol) without solvent at room temperature and t = 5 h.

5.3.3.2 Styrene epoxidation

Next, we explored the scope of extending the application of this catalyst system to alkene epoxidation, using the oxidation of styrene with hydrogen peroxide as a model reaction. Styrene being an electron-deficient species, its selective epoxidation over d^0 metal oxide catalysts is often regarded as a challenging reaction [14,33,47]. In the present study, on the other hand, we were pleased to find that the chitosan anchored peroxido-Nb(V) and peroxide-Ta(V) compounds could serve as highly potent catalysts in selective epoxidation of styrene under the solvent-free condition at room temperature.

Findings from our optimization study [**Table 5.6**, entry 1 and **Fig. 5.17**] demonstrated that, with a catalyst: substrate ratio of 1:100 and using 2 equivalents of H_2O_2, an impressive styrene conversion of 75% with >99% selectivity of the desired epoxide could be obtained at ambient temperature, without using any solvent. It was further possible to obtain a styrene conversion as high as 96% with nearly 100% epoxide selectivity and a reasonably good TON value of 96 [**Fig. 5.17** and **Table 5.6** (entry 4)] by increasing the H_2O_2 concentration from 2 to 4 equivalents. On raising the oxidant concentration further to 5 equivalents, overall styrene conversion declined (**Fig. 5.17**), as

has been observed in the case of phenol oxidation. Thus, styrene: H_2O_2 = 1:4 was considered optimal for styrene epoxidation, as well [**Fig. 5.17** and **Table 5.6** (entry 4)].
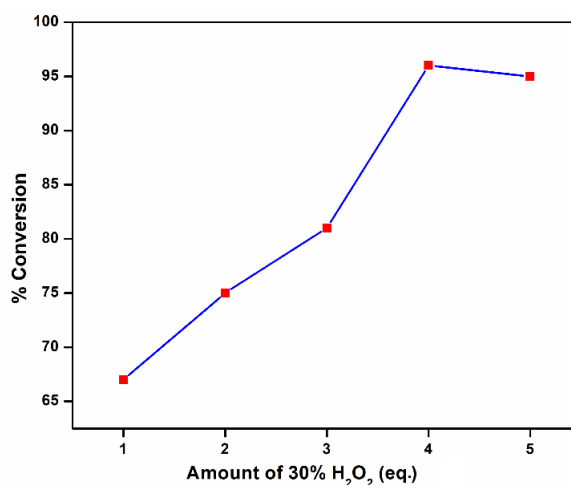
Fig. 5.17 Effect of H_2O_2 concentration on oxidation of styrene. Reaction conditions: Styrene (5 mmol), catalyst (0.05 mmol of Nb), RT, t = 8 h, without solvent.

On probing the reaction using different amounts of catalyst, it was observed that styrene conversion improved with an increment of the metal loading, as seen in **Fig. 5.18** and **Table 5.6** (entries 4,6-8). The reaction proceeded with nearly 100% epoxide selectivity in each case, although the resulting TON value decreased. Considering that the highest conversion of 96% could be obtained with a ratio of Nb: styrene of 1:100, this molar ratio was treated as optimal, although the maximum TON of 260 was observed at a considerably lower Nb: styrene molar ratio of 1:500 (**Table 5.6**, entry 6). The result of a
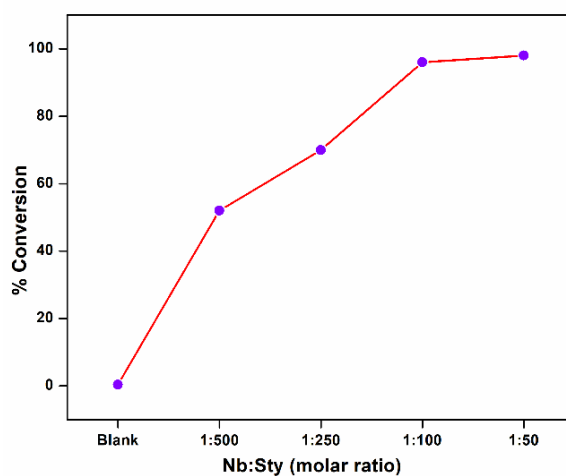
Fig. 5.18 Effect of catalyst loading on styrene oxidation. Reaction conditions: substrate (5 mmol), 30% H_2O_2 (20 mmol), room temperature, 8 h, without solvent.

control run carried out in catalyst-free condition showed <1% conversion of styrene (**Table 5.6**, entry 17). The observation once again testified to the indispensability of the catalyst in the present epoxidation process.

The styrene conversion *versus* reaction time profile presented in **Fig. 5.19** and the corresponding data listed in **Table 5.6** (entries 4, 9-13) show the trend obtained after monitoring the reaction over a period of 10 h. After the sharp rise in the styrene conversion within the initial period between 0.5-1 h of starting the reaction, the conversion of styrene increased gradually till 8 h (**Table 5.6**, **Fig. 5.19**). Thus, it is noteworthy that the reaction exhibited the best TOF of ~ 43 h^{-1} at the initial 1 h of the reaction time (**Table 5.6**, entry 10). Only a marginal increase in the styrene conversion was observed after extending the reaction beyond 8 h. Markedly, this observation is corroborating evidence that the catalyst is robust enough to retain its activity, along with the selectivity even up to 24 h of reaction time under the maintained reaction condition.
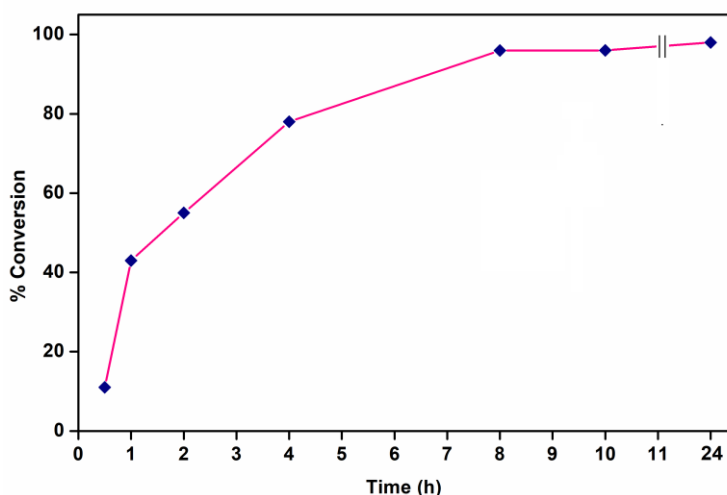
Fig. 5.19 Styrene conversion versus time. Reaction Conditions: 5 mmol of substrate, 30% H_2O_2 (20 mmol), catalyst (0.05 mmol of Nb), without solvent, RT.

We have also surveyed the solvent effect on the catalytic epoxidation protocol employing a variety of solvents, in addition to water. The results are presented in **Fig. 5.20**. Fulfilling our expectations, the catalyst performed efficiently in an aqueous medium as well as in other polar protic organic solvents to furnish nearly comparable styrene conversion of >89% along with >98% selectivity of epoxide [**Fig. 5.20**]. The observed high compatibility of the catalysts with water is in accord with a number of previous findings documenting high stability of Nb-based catalysts towards hydrolysis and metal

leaching, due to which such systems often displayed high efficiency in aqueous phase organic reactions [41,97,98].

Table 5.6: Optimization of reaction conditions for styrene epoxidation catalyzed by **ChpNb** (**5.1**)[a]

Styrene → Styrene oxide + Benzaldehyde (ChpNb, 30% H_2O_2, RT)

Entry	Molar ratio (Cat:Sty)	30% H_2O_2 (eq.)	Time (h)	Styrene conversion (%)	Epoxide selectivity (%)	TON
1	1:100	2	8	75	≥99	75
2	1:100	1	8	67	≥99	67
3	1:100	3	8	81	≥99	81
4	**1:100**	**4**	**8**	**96**	**≥99**	**96**
5	1:100	5	8	95	≥99	95
6	1:500	4	8	52	≥99	260
7	1:250	4	8	70	≥99	175
8	1:50	4	8	98	≥99	49
9	1:100	4	0.5	11	≥98	11
10	1:100	4	1	43	≥98	43
11	1:100	4	2	55	≥99	55
12	1:100	4	4	78	≥99	78
13	1:100	4	10	96	≥99	96
14	1:100	4	24	98	≥99	98
15[b]	1:100	4	8	94	≥98	94
16[c]	1:100	4	8	93	≥99	93
17[d]	-	4	8	0.4	≥99	-

[a]Reaction conditions: 5 mmol styrene, room temperature. [b]Results of scale-up reaction (5.2 g of substrate). [c]Conversion of 5th reaction cycle. [d]Blank reaction without any catalyst.
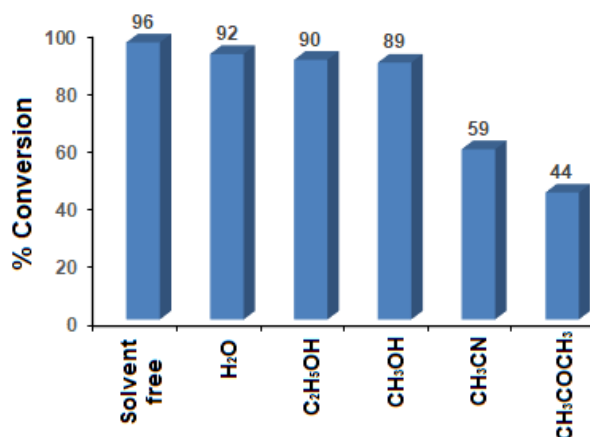
Fig. 5.20 Effect of solvent on styrene conversion. Reaction conditions: styrene (5 mmol), oxidant (20 mmol), catalyst (0.05 mmol of Nb), solvent (5 mL), RT, 8 h.

It is visible from the data depicted in **Fig. 5.21** that the chitosan immobilized peroxido-Ta(V) catalyst also exhibited excellent catalytic performance under optimized reaction conditions to selectively oxidize >91% of styrene to the corresponding epoxide with ≥ 99% selectivity and TON value of 91. Thus, in this case too, catalyst **ChpNb** performed relatively better in terms of styrene conversion, although with respect to epoxide selectivity, both the catalysts displayed comparable efficiency. As anticipated, the unsupported neat complexes $Na_3[Nb(O_2)_4]\cdot13H_2O$ and $Na_3[Ta(O_2)_4]\cdot H_2O$ with the same metal loading displayed poor styrene conversion (**Fig. 5.21**) as has been observed in the case of phenol hydroxylation.
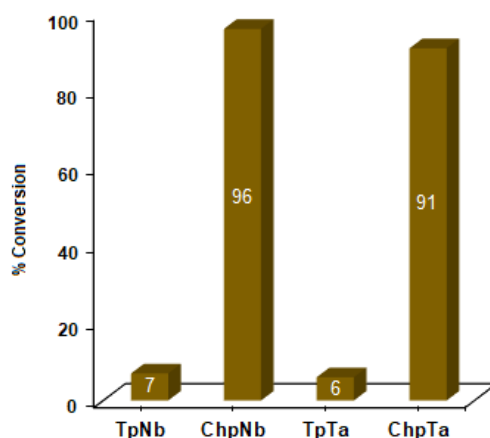
Fig. 5.21 Bar diagram showing the conversion of styrene by **ChpNb**, **ChpTa** along with the precursor complexes, $Na_3[Nb(O_2)_4]\cdot13H_2O$ and $Na_3[Ta(O_2)_4]\cdot H_2O$. [a]Reaction conditions: Styrene (5 mmol), catalyst (0.05 mmol of Nb or Ta), H_2O_2 (20 mmol) without solvent at room temperature and t = 8 h.

5.3.3.3 Sulfide oxidation

Encouraged by the above promising results, we have further directed our efforts towards implementing these catalyst systems in the sulfoxidation of thioethers. As shown in **Table 5.7** entry 1, preliminary experiments were carried out with thioanisole (MPS) and **ChpNb** as representative substrate and catalyst, respectively maintaining a Nb: MPS ratio of 1:1000 and MPS: H_2O_2 molar ratios of 1:2 under solventless condition at room temperature. Under these conditions, however, MPS was rapidly oxidized into a mixture of sulfoxide and sulfone. As the solvent-free method turned out to be non-selective, we have examined the reaction in the universal green solvent water. Finally, in an aqueous medium, it was possible to convert MPS quantitatively into pure sulfoxide with a TON of 970, within a reasonably short reaction time of 35 min, by maintaining Nb: MPS molar ratio of 1:1000 and using 3 equivalents of 30% H_2O_2 in a reaction conducted at ice bath temperature (**Table 5.7**, entry 4). It is indeed noteworthy that the methodology could provide a high TON value of 1900 even with a very low catalyst concentration (0.0025 mmol of Nb) (**Table 5.7**, entry 9). The catalysts also showed reasonably good activity in polar protic solvents, *viz.*, methanol and ethanol, albeit with a diminished sulfoxide selectivity, as the oxidation could not be stopped at sulfoxide level (**Table 5.7**, entries 10, 12). As in the case of phenol hydroxylation and styrene epoxidation, in this case too, the control reaction without any catalyst, as well as the oxidations conducted using the neat peroxidometallates as catalyst under optimized conditions, proceeded sluggishly, resulting in poor yield with a drop in sulfoxide selectivity [**Table 5.7**, entries 13, 14, 17].

The standardized catalytic protocol was then applied to a diverse range of sulfides such as aromatic, aliphatic, vinylic, allylic, and alcoholic sulfides in presence of each of the catalysts, **ChpNb** and **ChpTa.** Our findings listed in **Table 5.8** demonstrate that both the catalysts are highly active toward oxidation of the tested substrates to provide sulfoxide as the sole product under the optimized condition. The polymer-supported peroxidotantalum complex (**ChpTa**) also furnished competitive results, although at a relatively slower rate in comparison to Nb analog (**Table 5.7**, **5.8**).
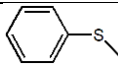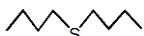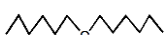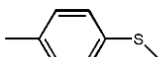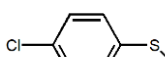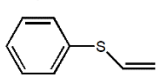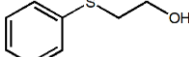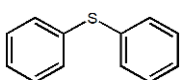
Table 5.7: Optimization of reaction conditions for sulfide oxidation by **ChpNb (5.1)**[a]

Entry	Molar ratio (Nb:MPS)	H_2O_2 (eq.)	Solvent	Time (min)	Isolated yield (%)	1a:1b	TON
1[b]	1:1000	2	-	20	98	53:47	980
2	1:1000	2	-	60	97	68:32	970
3	1:1000	3	-	40	98	65:35	980
4	**1:1000**	**3**	**H_2O**	**35**	**97**	**100:0**	**970**
5	1:1000	2	H_2O	60	95	80:20	950
6	1:1000	1	H_2O	80	96	85:15	960
7[c]	1:1000	3	H_2O	35	95	100:0	950
8	1:500	3	H_2O	35	96	100:0	480
9	1:2000	3	H_2O	90	95	100:0	1900
10	1:1000	3	MeOH	40	97	100:0	970
11	1:1000	3	MeCN	75	94	75:25	940
12	1:1000	3	EtOH	50	97	81:19	970
13[d]	1:1000	3	H_2O	35	18	73:27	180
14[e]	1:1000	3	H_2O	35	12	82:18	120
15[f]	1:1000	3	H_2O	60	98	100:0	980
16[g]	1:1000	3	H_2O	35	95	100:0	950
17[h]	-	3	H_2O	35	7	77:23	-

[a]All reactions were carried out with 5 mmol substrate, 5 mL solvent and at ice bath condition. [b]Reaction at room temperature. [c]Scaled-up reaction (6.2 g of MPS). [d]Reaction with $Na_3[Nb(O_2)_4]\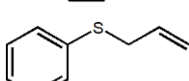cdot 13H_2O$ as catalyst (0.005 mmol). [e]Reaction with $Na_3[Ta(O_2)_4]\cdot H_2O$ as catalyst (0.005 mmol). [f]Reaction with **ChpTa** as a catalyst (0.005 mmol of Ta). [g]Conversion of 5th reaction cycle. [h]Blank reaction without catalyst.

Table 5.8: Selective oxidation of sulfides to sulfoxides with 30% H_2O_2 catalyzed by **ChpNb** (**5.1**) and **ChpTa** in presence of H_2O[a]

Entry	Substrate	ChpNb (5.1)			ChpTa		
		Time (min)	Isolated Yield (%)	TON	Time (min)	Isolated Yield (%)	TON
1		35	97	970	60	98	980
2		15	94	940	35	93	930
3		35	98	980	50	96	960
4		45	93	930	70	94	940
5		55	95	950	75	97	970
6		65	98	980	90	96	960
7		140	94	940	175	95	950
8		230	97	970	260	98	980
9		110	96	960	135	94	940
10		380	91	910	420	88	880

[a]Reaction conditions: Substrate (5 mmol), Catalyst (0.005 mmol of Nb or Ta), 30% H_2O_2 (15 mmol), H_2O (5 mL) at ice bath temperature.

The obtained data further revealed that aliphatic sulfides were oxidized more rapidly than the less nucleophilic conjugated ones, *viz.*, allylic, vinylic, or diphenyl sulfide (**Table 5.8**, entries 7,8,10), indicating that the rate of oxidation of sulfide with H_2O_2 is highly affected by the change in its nucleophilicity, induced by the presence of different substituents in it. Such a trend is not unexpected keeping in view that oxidation of sulfides is known to generally occur *via* the electrophilic addition of O atom [99,100]. Most importantly, both the catalysts displayed excellent chemoselectivity in the oxidation of sulfides having additional oxidation-prone C=C bond or -OH group (**Table 5.8**, entries 7-9).

5.3.3.4 Stability and reusability of the catalyst

The reusability of the catalysts was assessed individually for five successive cycles using styrene and MPS as substrates (**Fig. 5.22**). As the solid catalysts remained insoluble

during the course of the oxidation under the maintained reaction conditions, they were easily separable from the used reaction mixture by simple filtration or centrifugation. After washing with acetone and drying *in vacuo*, the recovered catalyst was used in a fresh run of oxidation under the respective optimized condition. The recyclability data presented in **Table 5.6** (entry 16) and **5.7** (entry 16) show that the activity and selectivity of the catalysts were preserved even after multiple cycles of reuse. In the case of phenol hydroxylation, however, catalyst reusability experiments could not be performed effectively, as difficulty was encountered in the separation and recovery of the catalysts from the organic products.
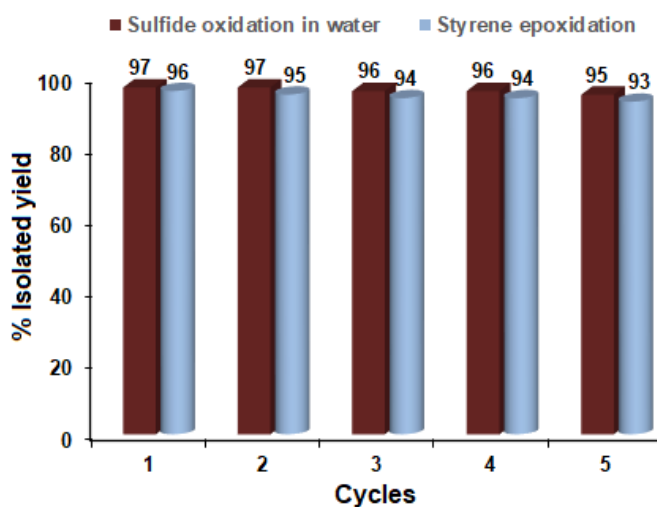
Fig. 5.22 Recyclability of the catalyst **ChpNb** (**5.1**) in sulfide oxidation and styrene epoxidation.

The recovered catalysts were subjected to FTIR, Raman, EDX, and powder XRD analyses in order to further confirm their stability during the catalytic process. The FTIR and Raman spectra, as well as PXRD patterns of the recovered catalysts resembled closely the patterns displayed by the respective original catalysts (**Fig. 5.23–5.25**). Furthermore, EDX analysis data showed no noticeable alteration in the metal content of the recovered catalysts compared to that of the starting catalysts. It is thus evident that the catalysts are sufficiently robust and capable of retaining their structural integrity during their reuse in repeated cycles of oxidations.
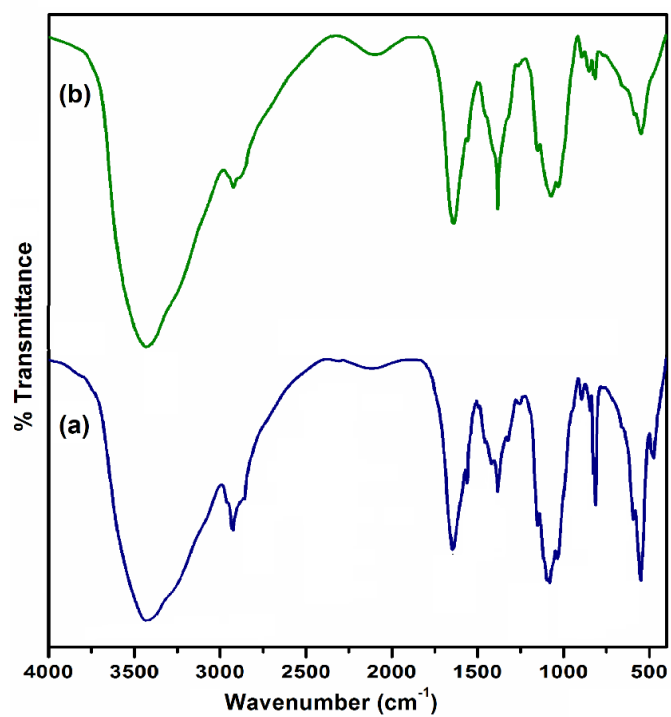
Fig. 5.23 FTIR spectra of (a) **ChpNb** and (b) **ChpNb** after 5th catalytic cycle.
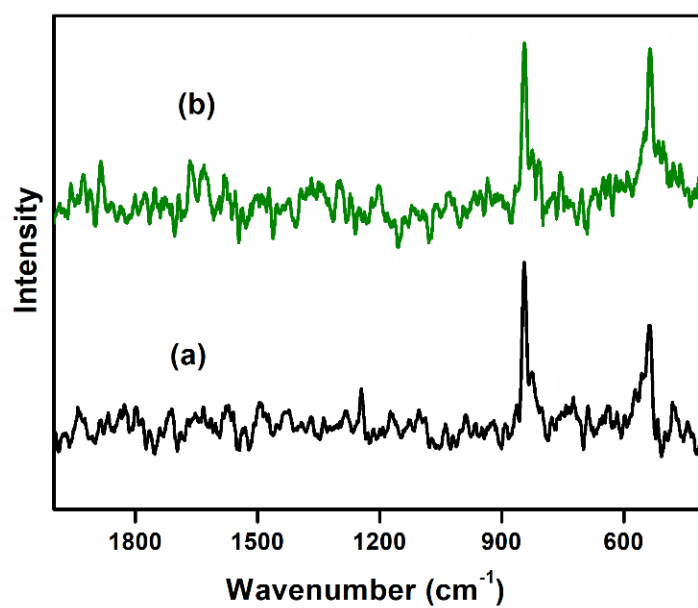
Fig. 5.24 Raman spectra of (a) fresh catalyst **ChpNb** and (b) recovered catalyst **ChpNb**.
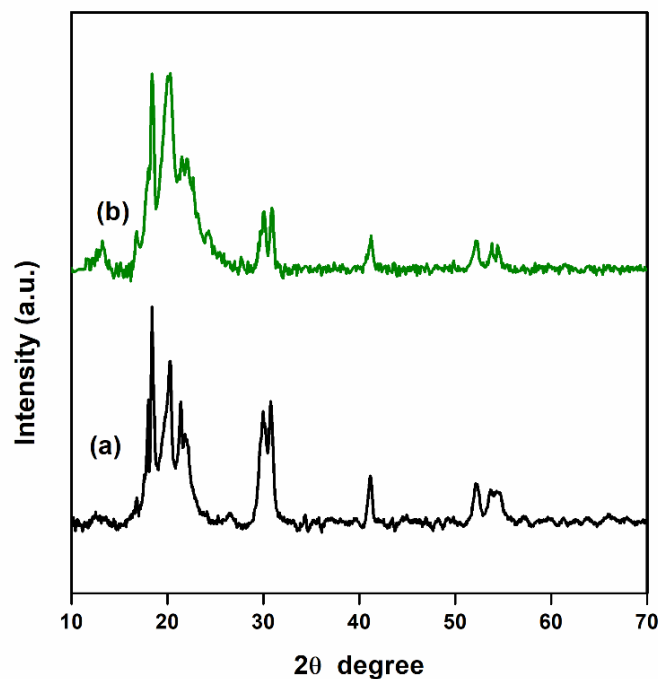
Fig. 5.25 PXRD patterns of (a) fresh catalyst **ChpNb** and (b) recovered catalyst **ChpNb**.

5.3.3.5 Heterogeneity test

To establish the heterogeneity of the aforementioned reactions catalyzed by the insoluble chitosan-supported solid catalysts**,** a standard hot filtration test was carried out under the respective optimized conditions. After attaining approximately 50% conversion of the substrate, as illustrated in **Fig. 5.26**, the solid catalyst was separated from the reaction mixture (after 2 h for styrene and 15 min for MPS), and the reaction was allowed to continue with the filtrate for a further period of 10 h in case of oxidation of styrene
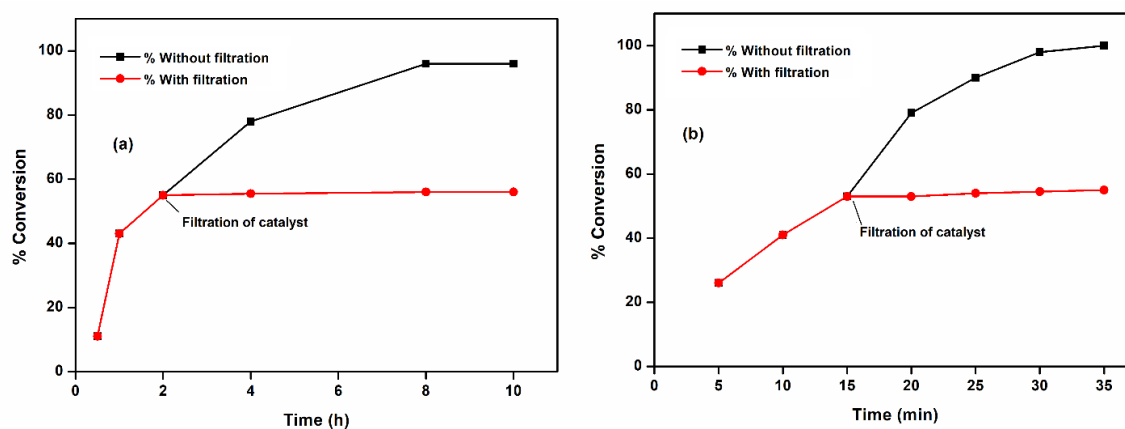
Fig. 5.26 Heterogeneity test for (a) styrene epoxidation and (b) sulfide oxidation in water catalyzed by **ChpNb** (**5.1**).

(35 min for MPS). The conversion of styrene or MPS did not improve after the separation of the catalyst, signifying the truly heterogeneous behaviour of the catalyst systems. Furthermore, when the filtrate was subjected to ICP-OES analysis no indication of the presence of Nb or Ta was found in it. It can thus be concluded that there was no leaching of catalytically active peroxidometal species from the support.

5.3.3.6 Scalability of the catalytic methodologies

To ascertain the scope of each of the aforementioned procedures for relatively larger-scale applications, we conducted the reactions at a ten-fold scale (phenol = 4.7 g; styrene = 5.2 g; MPS = 6.2 g), keeping the metal: substrate and substrate: oxidant molar ratios same as the respective optimized conditions. The results tabulated in **Table 5.5** (entry 13), **5.6** (entry 15), and **5.7** (entry 7) for all the three oxidation processes, *viz*. phenol hydroxylation, styrene epoxidation and sulfide oxidation, indicated that the developed catalytic procedures are amenable to scalability.

5.3.3.7 Comparison with some reported catalysts

An analysis of the comparative data depicted in **Table 5.9**, revealed that the catalytic performance of the present catalyst systems compares well with those of existing best Nb or Ta-based heterogeneous catalytic procedures conducted in various organic solvents with respect to each of the oxidation reactions examined [33,35,44,47,52-56,101-103]. In fact, the present solvent-free epoxidation protocol showed significantly superior performance in H_2O_2 induced styrene epoxidation in terms of both styrene conversion as well as epoxide selectivity [33,44,47,52]. Similarly, relatively better results were also observed in case of phenol hydroxylation in comparison to those obtained with niobium catalysts supported on mesoporous molecular sieves [53,54,56,101]. Further, catalysts provided competitive results in aqueous phase selective sulfoxidation reaction comparable to the reported Nb or Ta-based heterogeneous catalytic procedures conducted in organic solvents [35,54,102,103]. An additional noteworthy advantage of the present catalysts is the ease of recyclability with nearly undiminished activity and selectivity for multiple cycles of epoxidation and sulfoxidation. In case of most of the silica-supported or other oxide-based Nb catalysts, the recovered catalyst was usually needed to be reactivated by calcination prior to reuse in subsequent oxidation [33,44,47,54]. Above all, our conditions

Table 5.9: The catalytic activity of **ChpNb** and **ChpTa** *vis-à-vis* some reported supported Nb or Ta-based catalysts in phenol hydroxylation, styrene epoxidation and sulfide oxidation

Entry	Catalyst	Substrate	Catalyst amount	Reaction conditions	% Conversion/ % Selectivity[a-c]	Ref
1	**ChpNb**	**Styrene**	**0.05 mmol**	**8 h, RT, H$_2$O$_2$, Solventless**	**96/>99**	**This work**
2	**ChpTa**	**Styrene**	**0.05 mmol**	**8 h, RT, H$_2$O$_2$, Solventless**	**91/>99**	**This work**
3	Calix-Nb-SiO$_2$	Styrene	0.00102 M	6 h, 65 ºC, H$_2$O$_2$, MeCN	53/20	[33]
4	Nb-KIT-5(10)	Styrene	20 mg	6 h, 50 ºC, H$_2$O$_2$, MeOH	51/13	[47]
5	Nb-MMM-E	Styrene	0.005 mmol	1 h, 50 ºC, H$_2$O$_2$, MeCN	20/50	[44]
6	DET-Ta-MCM650	Styrene	0.015 mmol	24 h, 70 ºC, TBHP, CH$_3$CN	73/34	[52]
7	Ta–SiO$_2$	Styrene	0.01 mmol	6 h, 65 ºC, H$_2$O$_2$, CH$_3$CN	37/36	[33]
8	**ChpNb**	**Phenol**	**0.1 mmol**	**5 h, RT, H$_2$O$_2$, Solventless**	**35/100**	**This work**
9	FeNbMCM-41-64	Phenol	0.2 g	2 h 40 min, 60ºC, H$_2$O$_2$, H$_2$O	24/1.29	[101]
10	[Nb$_{1.0}$(PO$_4$)$_{1.0}$](HPO$_4$)$_{0.13}$Cl$_{0.74}$	Phenol	0.1 g	15 h, 80ºC, H$_2$O$_2$, MeOH	15.3/99.8	[55]
11	NbPMOs	Phenol	--	--, H$_2$O$_2$, H$_2$O	15/100	[53]
12	NbVMCM-41-32	Phenol	0.2 g	5 h, 80ºC, H$_2$O$_2$, H$_2$O	2.55/100	[54]

Continued…

Entry	Catalyst	Substrate	Catalyst amount	Reaction conditions	% Conversion/ % Selectivity[a-c]	Ref
13	**ChpNb**	**MPS**	**0.005 mmol**	**0.58 h, ice bath, H_2O_2, H_2O**	**100/100**	**This work**
14	**ChpTa**	**MPS**	**0.005 mmol**	**1 h, ice bath, H_2O_2, H_2O**	**100/100**	**This work**
15	NbVMCM-41-32	MPS	0.04 g	2 h, 50°C, H_2O_2, MeOH	98/100	[54]
16	0.25-PPA-Nb-SiO$_2$	MPS	0.01 mmol	0.25 h, 45 °C, H_2O_2, MeCN	65/78	[102]
17	TaC	MPS	0.02 equiv.	1.25 h, 45 °C, H_2O_2, MeOH	100/99	[103]
18	Modified Ta-MCM with DIPT	MPS	0.012 mmol	24 h, RT, H_2O_2, MeOH	85/90	[35]

[a]Selectivity of dihydroxybenzene. [b]Epoxide selectivity. [c]Methyl phenyl sulfoxide selectivity.

are milder and environmentally friendly since all the oxidation reactions in the present study were conducted without the addition of organic solvent, at natural pH of the reaction medium, in absence of any acid, halide, or any other non-green additives.

5.3.3.8 Proposed catalytic cycle

The plausible catalytic cycles envisaged for all the three oxidation processes, *viz.*, styrene epoxidation, phenol hydroxylation and sulfide oxidation, are illustrated in **Scheme 5.1**. It has been well documented in the literature that direct oxygen transfer from the peroxido group bound to various group V and VI metals to a nucleophilic substrate generally occurs *via* a common pathway involving a simple bimolecular interaction between the metal peroxide and the nucleophile [104-106]. Although the activity of pre-formed peroxido complexes of Nb(V) and Ta(V) in organic oxidation has not been explored abundantly, a number of reports are available dealing with the mode of olefin epoxidation with H_2O_2 over Nb and Ta-oxide based solid catalysts [46,104,105,107-109].

Based on the observations from our present work and taking into account the above information, it is expected that in the first step of styrene epoxidation (**Scheme 5.1**, **cycle A**), the transfer of electrophilic O atom from the active peroxido group of chitosan bound Nb(V) or Ta(V) complexes to styrene would take place (**reaction a**) to yield the desired epoxide. The oxygen transfer is accompanied by the formation of oxidodiperoxido intermediate species **II**. The oxidodiperoxido intermediate of Nb(V) or Ta(V) would then react with H_2O_2 in the next step (**reaction b**) to regenerate the original catalyst. In a similar line, as shown in catalytic **cycle B**, transfer of oxygen to phenol from the triperoxidometallate group of the catalyst would occur to afford the hydroxylated products CT and HQ (**reaction c**). The proposed catalytic cycle (**cycle C**) for the oxidation of organic sulfides to sulfoxides (**reaction e**) is also depicted in **Scheme 5.1**, which is consistent with the well-established mechanism of sulfoxidation reaction catalyzed by various peroxidometallates [97-99,110-112]. There have been several reports implicating the involvement of an oxidoperoxidoniobium(V) intermediate of the type **II** during the process of oxygen transfer from an active peroxidoniobium complex to an organic substrate [72,97,98,113]. Although, at this stage we do not have further data to suggest more detailed mechanisms, the proposed catalytic cycles are in accord with previous findings from a number of laboratories,

including ours, pertaining to olefin epoxidation and sulfide oxidation by Nb(V) and Ta(V) peroxide systems [97,98,113,114].
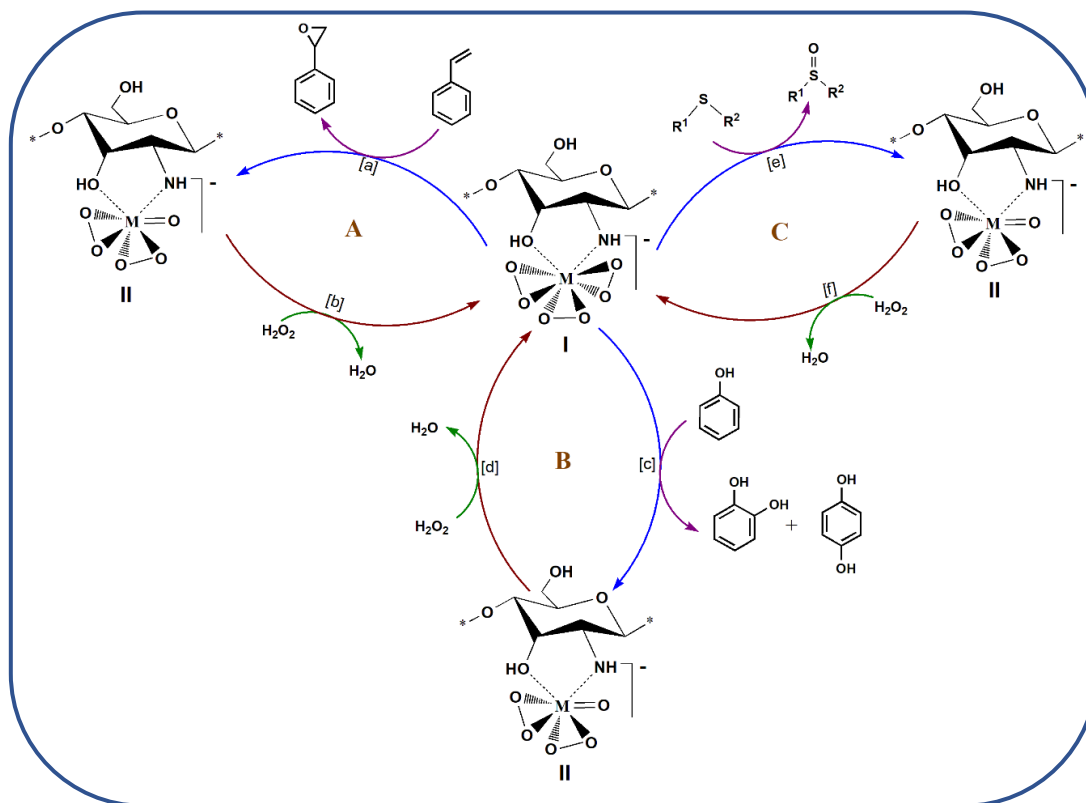
Scheme 5.1 Proposed catalytic cycle for A. epoxidation of styrene, B. hydroxylation of phenol and C. oxidation of sulfides to sulfoxides (M = Nb or Ta). " * " represents polymer chain.

5.4 Conclusions

In summary, the triperoxido derivative of Nb(V) and Ta(V) supported on chitosan have emerged as robust and versatile heterogenized catalyst system, applicable in a variety of organic oxidations. The catalysts displayed outstanding efficiency in oxidizing styrene with H_2O_2 almost quantitatively to the desired epoxide with 100% selectivity under the non-solvent condition at room temperature. Moreover, one-step oxidation of phenol could be achieved in presence of these catalysts at ambient temperature with 100% dihydroxybenzene selectivity (HQ: CT ratio of *ca* 2:1) without the addition of any solvent. Interestingly, the catalysts could perform these oxidations in the aqueous medium as well. The versatility of the immobilized compounds as water compatible and water tolerant catalysts was further revealed by their efficiency in promoting the oxidation of a broad range of sulfides

chemoselectively to the targeted sulfoxides in the eco-friendly solvent, water. Additional salient features which considerably enhance the environmental sustainability and synthetic utility of the methodologies include: (i) the oxidation protocols are free from toxic solvents, hazardous additives or by-products; (ii) all the results were achieved using H_2O_2 as green oxidant, without involving elevated temperature; (iii) catalysts were obtained *via* a simple preparation protocol using non-toxic metal and cheap, abundant renewable material as support. Furthermore, the ready scalability of the catalysts and their easy recyclability at least up to five successive cycles of epoxidation and sulfoxidation, with virtually no loss in catalytic activity, are significant strengths of the developed catalytic procedures, which make them potentially useful for practical implementation.

References

1. Nasrollahzadeh, M., Shafiei, N., Nezafat, Z., Bidgoli, N. S. S., and Soleimani, F. Recent progresses in the application of cellulose, starch, alginate, gum, pectin, chitin and chitosan based (nano) catalysts in sustainable and selective oxidation reactions: A review. *Carbohydrate Polymers*, 241:116353, 2020.

2. Molnár, Á. The use of chitosan-based metal catalysts in organic transformations. *Coordination Chemistry Reviews*, 388:126-171, 2019.

3. Jiménez-Gómez, C. P. and Cecilia, J. A. Chitosan: A natural biopolymer with a wide and varied range of applications. *Molecules*, 25(17):3981, 2020.

4. Balakrishnan, A., Appunni, S., Chinthala, M., and Vo, D.-V. N. Biopolymer-supported TiO_2 as a sustainable photocatalyst for wastewater treatment: A review. *Environmental Chemistry Letters*, 20(5):3071-3098, 2022.

5. Wang, X., Hu, P., Xue, F., and Wei, Y. Cellulose-supported N-heterocyclic carbene-palladium catalyst: Synthesis and its applications in the Suzuki cross-coupling reaction. *Carbohydrate Polymers*, 114:476-483, 2014.

6. Wang, X., Du, Y., and Liu, H. Preparation, characterization and antimicrobial activity of chitosan–Zn complex. *Carbohydrate Polymers*, 56(1):21-26, 2004.

7. Hamed, I., Özogul, F., and Regenstein, J. M. Industrial applications of crustacean by-products (chitin, chitosan, and chitooligosaccharides): A review. *Trends in Food Science & Technology*, 48:40-50, 2016.

8. Varma, A., Deshpande, S., and Kennedy, J. Metal complexation by chitosan and its derivatives: A review. *Carbohydrate Polymers*, 55(1):77-93, 2004.

9. Omer, A. M., Dey, R., Eltaweil, A. S., Abd El-Monaem, E. M., and Ziora, Z. M. Insights into recent advances of chitosan-based adsorbents for sustainable removal of heavy metals and anions. *Arabian Journal of Chemistry*, 15(2):103543, 2022.

10. Lee, D. N., Gwon, K., Nam, Y., Lee, S. J., Tran, N. M., and Yoo, H. Polyurethane foam incorporated with nanosized copper-based metal-organic framework: Its antibacterial properties and biocompatibility. *International Journal of Molecular Sciences*, 22(24):13622, 2021.

11. Sakthivel, B. and Dhakshinamoorthy, A. Chitosan as a reusable solid base catalyst for Knoevenagel condensation reaction. *Journal of Colloid and Interface Science*, 485:75-80, 2017.

12. Zhu, J., Wang, P. C., and Lu, M. Synthesis of novel magnetic chitosan supported protonated peroxotungstate and its catalytic performance for oxidation. *New Journal of Chemistry*, 36(12):2587-2592, 2012.

13. Zhu, J., Zhao, X. J., Wang, P. C., and Lu, M. Green oxidation process in the synthesis of LLM-105 with H_2O_2/peroxotungstate system and its theoretical study. *Journal of Heterocyclic Chemistry*, 53(5):1386-1394, 2016.

14. Yan, W., Zhang, G., Yan, H., Liu, Y., Chen, X., Feng, X., Jin, X., and Yang, C. Liquid-phase epoxidation of light olefins over W and Nb nanocatalysts. *ACS Sustainable Chemistry & Engineering*, 6(4):4423-4452, 2018.

15. Bauer, K., Garbe, D., and Surburg, H. *Common Fragrance and Flavor Materials: Preparation, Properties and Uses*. John Wiley & Sons, 2008.

16. Legros, J., Dehli, J. R., and Bolm, C. Applications of catalytic asymmetric sulfide oxidations to the syntheses of biologically active sulfoxides. *Advanced Synthesis & Catalysis*, 347(1):19-31, 2005.

17. Maurya, M. R. and Sikarwar, S. Oxidation of phenol and hydroquinone catalysed by copper(II) and oxovanadium(IV) complexes of N, N′-bis (salicyledene) diethylenetriamine (H_2saldien) covalently bonded to chloromethylated polystyrene. *Journal of Molecular Catalysis A: Chemical*, 263(1-2):175-185, 2007.

18. Nohl, H., Jordan, W., and Youngman, R. J. Quinones in biology: functions in electron transfer and oxygen activation. *Advances in Free Radical Biology & Medicine*, 2(1):211-279, 1986.

19. Caron, S., Dugger, R. W., Ruggeri, S. G., Ragan, J. A. and Ripin, D. H. B. Large-scale oxidations in the pharmaceutical industry. *Chemical Reviews*, 106(7):2943-2989, 2006.

20. Atoguchi, T., Kanougi, T., Yamamoto, T., and Yao, S. Phenol oxidation into catechol and hydroquinone over H-MFI, H-MOR, H-USY and H-BEA in the presence of ketone. *Journal of Molecular Catalysis A: Chemical*, 220(2):183-187, 2004.

21. Zhang, Y., Xiao, S., Xie, J., Yang, Z., Pang, P., and Gao, Y. Simultaneous electrochemical determination of catechol and hydroquinone based on graphene–TiO_2 nanocomposite modified glassy carbon electrode. *Sensors and Actuators B: Chemical*, 204:102-108, 2014.

22. Santos, A., Yustos, P., Quintanilla, A., Rodrıguez, S., and Garcıa-Ochoa, F. Route of the catalytic oxidation of phenol in aqueous phase. *Applied Catalysis B: Environmental*, 39(2):97-113, 2002.

23. Hai, L., Zhang, T., Zhang, X., Zhang, G., Li, B., Jiang, S., and Ma, X. Catalytic hydroxylation of phenol to dihydroxybenzene by Fe(II) complex in aqueous phase at ambient temperature. *Catalysis Communications*, 101:93-97, 2017.

24. Maurya, M. R., Kumar, A., and Pessoa, J. C. Vanadium complexes immobilized on solid supports and their use as catalysts for oxidation and functionalization of alkanes and alkenes. *Coordination Chemistry Reviews*, 255(19-20):2315-2344, 2011.

25. Adam, F., Wong, J.-T., and Ng, E.-P. Fast catalytic oxidation of phenol over iron modified zeolite L nanocrystals. *Chemical Engineering Journal*, 214:63-67, 2013.

26. De Faveri, G., Ilyashenko, G., and Watkinson, M. Recent advances in catalytic asymmetric epoxidation using the environmentally benign oxidant hydrogen peroxide and its derivatives. *Chemical Society Reviews*, 40(3):1722-1760, 2011.

27. Sherrington, D. C. Polymer-supported metal complex alkene epoxidation catalysts. *Catalysis Today*, 57(1-2):87-104, 2000.

28. Kholdeeva, O. A. Recent developments in liquid-phase selective oxidation using environmentally benign oxidants and mesoporous metal silicates. *Catalysis Science & Technology*, 4(7):1869-1889, 2014.

29. Salazar-Aguilar, A. D., Vega, G., Casas, J. A., Vega-Díaz, S. M., Tristan, F., Meneses-Rodríguez, D., Belmonte, M., and Quintanilla, A. Direct hydroxylation of phenol to dihydroxybenzenes by H_2O_2 and Fe-based metal-organic framework catalyst at room temperature. *Catalysts*, 10(2):172, 2020.

30. Batra, M. S., Dwivedi, R., and Prasad, R. Recent developments in heterogeneous catalyzed epoxidation of styrene to styrene oxide. *ChemistrySelect*, 4(40):11636-11673, 2019.

31. Sharma, A. S., Sharma, V. S., Kaur, H., and Varma, R. S. Supported heterogeneous nanocatalysts in sustainable, selective and eco-friendly epoxidation of olefins. *Green Chemistry*, 22(18):5902-5936, 2020.

32. Noyori, R., Aoki, M., and Sato, K. Green oxidation with aqueous hydrogen peroxide. *Chemical Communications*, (16):1977-1986, 2003.

33. Thornburg, N. E., Thompson, A. B., and Notestein, J. M. Periodic trends in highly dispersed groups IV and V supported metal oxide catalysts for alkene epoxidation with H_2O_2. *ACS Catalysis*, 5(9):5077-5088, 2015.

34. Tiozzo, C., Bisio, C., Carniato, F., and Guidotti, M. Grafted non-ordered niobium-silica materials: Versatile catalysts for the selective epoxidation of various unsaturated fine chemicals. *Catalysis Today*, 235:49-57, 2014.

35. Fadhli, M., Khedher, I., and Fraile, J. M. Modified Ta/MCM-41 catalysts for enantioselective oxidation of thioanisole. *Journal of Molecular Catalysis A: Chemical*, 410:140-148, 2015.

36. Guillo, P., Lipschutz, M. I., Fasulo, M. E., and Tilley, T. D. Tantalum–polyhedral oligosilsesquioxane complexes as structural models and functional catalysts for epoxidation. *ACS Catalysis*, 7(4):2303-2312, 2017.

37. Ruddy, D. A., Brutchey, R. L., and Tilley, T. D. The influence of surface modification on the epoxidation selectivity and mechanism of TiSBA15 and TaSBA15 catalysts with aqueous hydrogen peroxide. *Topics in Catalysis*, 48(1):99-106, 2008.

38. Gallo, A., Tiozzo, C., Psaro, R., Carniato, F., and Guidotti, M. Niobium metallocenes deposited onto mesoporous silica via dry impregnation as catalysts for selective epoxidation of alkenes. *Journal of Catalysis*, 298:77-83, 2013.

39. Black, J. Biologic performance of tantalum. *Clinical Materials*, 16(3):167-173, 1994.

40. Olivares-Navarrete, R., Olaya, J. J., Ramírez, C., and Rodil, S. E. Biocompatibility of niobium coatings. *Coatings*, 1(1):72-87, 2011.

41. Ziolek, M. Niobium-containing catalysts—the state of the art. *Catalysis Today*, 78(1-4):47-64, 2003.

42. Selvaraj, M., Kawi, S., Park, D., and Ha, C. A merit synthesis of well-ordered two-dimensional mesoporous niobium silicate materials with enhanced hydrothermal stability and catalytic activity. *Journal of Physical Chemistry C*, 113(18):7743-7749, 2009.

43. Gallo, J. M. R., Paulino, I. S., and Schuchardt, U. Cyclooctene epoxidation using Nb-MCM-41 and Ti-MCM-41 synthesized at room temperature. *Applied Catalysis A- General*, 266(2):223-227, 2004.

44. Ivanchikova, I. D., Maksimchuk, N. V., Skobelev, I. Y., Kaichev, V. V., and Kholdeeva, O. A. Mesoporous niobium-silicates prepared by evaporation-induced self-assembly as catalysts for selective oxidations with aqueous H_2O_2. *Journal of Catalysis*, 332:138-148, 2015.

45. Tiozzo, C., Bisio, C., Carniato, F., Gallo, A., Scott, S. L., Psaro, R., and Guidotti, M. Niobium–silica catalysts for the selective epoxidation of cyclic alkenes: the generation of the active site by grafting niobocene dichloride. *Physical Chemistry Chemical Physics*, 15(32):13354-13362, 2013.

46. Ivanchikova, I. D., Skobelev, I. Y., Maksimchuk, N. V., Paukshtis, E. A., Shashkov, M. V., and Kholdeeva, O. A. Toward understanding the unusual reactivity of mesoporous niobium silicates in epoxidation of C=C bonds with hydrogen peroxide. *Journal of Catalysis*, 356:85-99, 2017.

47. Ramanathan, A., Maheswari, R., and Subramaniam, B. Facile styrene epoxidation with H_2O_2 over novel niobium containing cage type mesoporous silicate, Nb-KIT-5. *Topics in Catalysis*, 58(4):314-324, 2015.

48. Somma, F., Canton, P., and Strukul, G. Effect of the matrix in niobium-based aerogel catalysts for the selective oxidation of olefins with hydrogen peroxide. *Journal of Catalysis*, 229(2):490-498, 2005.

49. Ruddy, D. A. and Tilley, T. D. Highly selective olefin epoxidation with aqueous H_2O_2 over surface-modified TaSBA15 prepared via the TMP method. *Chemical Communications*, (32):3350-3352, 2007.

50. Morlanés, N. and Notestein, J. M. Grafted Ta–calixarenes: Tunable, selective catalysts for direct olefin epoxidation with aqueous hydrogen peroxide. *Journal of Catalysis*, 275(2):191-201, 2010.

51. Cordeiro, P. J. and Tilley, T. D. Enhancement of epoxidation efficiencies for Ta-SBA15 catalysts. The influence of modification with–EMe_3 (E= Si, Ge, Sn) Groups. *Langmuir*, 27(10):6295-6304, 2011.

52. Fadhli, M., Khedher, I., and Fraile, J. M. Comparison of Ta–MCM-41 and Ti–MCM-41 as catalysts for the enantioselective epoxidation of styrene with TBHP. *Comptes Rendus Chimie*, 20(8):827-832, 2017.

53. Nowak, I. and Walczak, K. *Niobium-Induced Synthesis of SBA-15 Type Nioboorganosilicates-Oxidation Catalyst*.

54. Ziolek, M., Lewandowska, A., Renn, M., and Nowak, I. The use of niobium containing mesoporous molecular sieves in the liquid phase oxidation. *Studies in Surface Science and Catalysis*, 154:2610-2617, 2004.

55. Mal, N. K., Bhaumik, A., Kumar, P., and Fujiwara, M. Microporous niobium phosphates and catalytic properties prepared by a supramolecular templating mechanism. *Chemical Communications*, (7):872-873, 2003.

56. Sobczak, I., Ziolek, M., Renn, M., Decyk, P., Nowak, I., Daturi, M., and Lavalley, J.-C. Cu state and behaviour in MCM-41 mesoporous molecular sieves modified with copper during the synthesis--comparison with copper exchanged materials. *Microporous and Mesoporous Materials*, 74(1-3):23-36, 2004.

57. Saikia, G. *Synthesis and Characterization of Polymer Anchored Compounds of Vanadium(V) and Tantalum(V). Exploration of Their Catalytic and Biochemical Potential.* PhD thesis, Department of Chemical Sciences, Tezpur University, 2020.

58. Saikia, G., Ahmed, K., Gogoi, S. R., Sharma, M., Talukdar, H., and Islam, N. S. A chitosan supported peroxidovanadium(V) complex: Synthesis, characterization and application as an eco-compatible heterogeneous catalyst for selective sulfoxidation in water. *Polyhedron*, 159:192-205, 2019.

59. Ahmed, K., Saikia, G., Begum, P., Gogoi, S. R., Sharma, M., Talukdar, H., and Islam, N. S. Selective and green sulfoxidation in water using a new chitosan supported Mo(VI) complex as heterogeneous catalyst. *ChemistrySelect*, 3(44):12563-12575, 2018.

60. Negm, N. A., Hefni, H. H., Abd-Elaal, A. A., Badr, E. A., and Abou Kana, M. T. Advancement on modification of chitosan biopolymer and its potential applications. *International Journal of Biological Macromolecules*, 152:681-702, 2020.

61. Trimukhe, K. and Varma, A. A morphological study of heavy metal complexes of chitosan and crosslinked chitosans by SEM and WAXRD. *Carbohydrate Polymers*, 71(4):698-702, 2008.

62. Ou, C., Li, S., Shao, J., Fu, T., Liu, Y., Fan, W., Yang, X., and Bi, X. Effect of transition metal ions on the thermal degradation of chitosan. *Cogent Chemistry*, 2(1):1216247, 2016.

63. Mondéjar-López, M., Rubio-Moraga, A., López-Jimenez, A. J., Martínez, J. C. G., Ahrazem, O., Gómez-Gómez, L., and Niza, E. Chitosan nanoparticles loaded with garlic essential oil: A new alternative to tebuconazole as seed dressing agent. *Carbohydrate Polymers*, 277:118815, 2022.

64. Hussein, M., El-Hady, M., Sayed, W., and Hefni, H. Preparation of some chitosan heavy metal complexes and study of its properties. *Polymer Science, Series A*, 54(2):113-124, 2012.

65. García-Sancho, C., Sádaba, I., Moreno-Tost, R., Mérida-Robles, J., Santamaría-González, J., López-Granados, M., and Maireles-Torres, P. Dehydration of xylose to furfural over MCM-41-supported niobium-oxide catalysts. *ChemSusChem*, 6(4):635-642, 2013.

66. Atashbar, M., Sun, H., Gong, B., Wlodarski, W., and Lamb, R. XPS study of Nb-doped oxygen sensing TiO_2 thin films prepared by sol-gel method. *Thin Solid Films*, 326(1-2):238-244, 1998.

67. Brunauer, S., Emmett, P. H., and Teller, E. Adsorption of gases in multimolecular layers. *Journal of the American Chemical Society*, 60(2):309-319, 1938.

68. Barrett, E. P., Joyner, L. G., and Halenda, P. P. The determination of pore volume and area distributions in porous substances. I. Computations from nitrogen isotherms. *Journal of the American Chemical Society,* 73(1):373-380, 1951.

69. Sing, K. S. W., Everett, D., Haul, R., Moscou, L., Pierotti, R., Rouquerol, J., and Siemieniewska, T. International union of pure commission on colloid and surface chemistry including catalysis* reporting physisorption data for gas/solid systems with special reference to the determination of surface area and porosity. *Pure and Applied Chemistry*, 57(4):603-619, 1985.

70. Thommes, M., Kaneko, K., Neimark, A. V., Olivier, J. P., Rodriguez-Reinoso, F., Rouquerol, J., and Sing, K. S. Physisorption of gases, with special reference to the evaluation of surface area and pore size distribution (IUPAC Technical Report). *Pure and Applied Chemistry*, 87(9-10):1051-1069, 2015.

71. Alkhamis, K. A., Salem, M. S., and Khanfar, M. S. The sorption of ketotifen fumarate by chitosan. *AAPS PharmSciTech*, 9(3):866-869, 2008.

72. Bayot, D. and Devillers, M. Peroxo complexes of niobium(V) and tantalum(V). *Coordination Chemistry Reviews*, 250(19-20):2610-2626, 2006.

73. Djordjevic, C. and Vuletic, N. Coordination complexes of niobium and tantalum. V. Eight-coordinated di-and triperoxoniobates(V) and-tantalates(V) with some nitrogen and oxygen bidentate ligands. *Inorganic Chemistry*, 7(9):1864-1868, 1968.

74. Bayot, D., Devillers, M., and Peeters, D. Vibrational spectra of eight-coordinate niobium and tantalum complexes with peroxo ligands: A theoretical simulation. *European Journal of Inorganic Chemistry*, 4118–4123, 2005.

75. Dimzon, I. K. D. and Knepper, T. P. Degree of deacetylation of chitosan by infrared spectroscopy and partial least squares. *International Journal of Biological Macromolecules*, 72:939-945, 2015.

76. AbdElhady, M. Preparation and characterization of chitosan/zinc oxide nanoparticles for imparting antimicrobial and UV protection to cotton fabric. *International Journal of Carbohydrate Chemistry*, 2012, 2012.

77. Fei Liu, X., Lin Guan, Y., Zhi Yang, D., Li, Z., and De Yao, K. Antibacterial action of chitosan and carboxymethylated chitosan. *Journal of Applied Polymer Science*, 79(7):1324-1335, 2001.

78. Maniatakou, A., Makedonas, C., Mitsopoulou, C. A., Raptopoulou, C., Rizopoulou, I., Terzis, A., and Karaliota, A. Synthesis, structural and DFT studies of a peroxo-niobate complex of the biological ligand 2-quinaldic acid. *Polyhedron*, 27(16):3398-3408, 2008.

79. Narendar, Y. and Messing, G. L. Synthesis, decomposition and crystallization characteristics of peroxo-citrato-niobium: An aqueous niobium precursor. *Chemistry of Materials*, 9(2):580-587, 1997.

80. Wang, Y., Pitto-Barry, A., Habtemariam, A., Romero-Canelon, I., Sadler, P. J., and Barry, N. P. Nanoparticles of chitosan conjugated to organo-ruthenium complexes. *Inorganic Chemistry Frontiers*, 3(8):1058-1064, 2016.

81. Guibal, E., Milot, C., Eterradossi, O., Gauffier, C., and Domard, A. Study of molybdate ion sorption on chitosan gel beads by different spectrometric analyses. *International Journal of Biological Macromolecules*, 24(1):49-59, 1999.

82. Modrzejewska, Z., Dorabialska, M., Zarzycki, R., and Wojtasz-Pająk, A. The mechanism of sorption of Ag^+ ions on chitosan microgranules: IR and NMR studies. *Progress on Chemistry and Application of Chitin and its Derivatives*, 14:49-64, 2009.

83. Wei, X., Chen, S., Rong, J., Sui, Z., Wang, S., Lin, Y., Xiao, J., and Huang, D. Improving the Ca(II) adsorption of chitosan via physical and chemical modifications and charactering the structures of the calcified complexes. *Polymer Testing*, 98:107192, 2021.

84. Wu, T., Wu, C., Xiang, Y., Huang, J., Luan, L., Chen, S., and Hu, Y. Kinetics and mechanism of degradation of chitosan by combining sonolysis with H_2O_2/ascorbic acid. *RSC Advances*, 6(80):76280-76287, 2016.

85. Ramya, R., Sudha, P., and Mahalakshmi, J. Preparation and characterization of chitosan binary blend. *International Journal of Scientific and Research Publications*, 2(10):1-9, 2012.

86. Rhazi, M., Desbrieres, J., Tolaimate, A., Rinaudo, M., Vottero, P., Alagui, A., and El Meray, M. Influence of the nature of the metal ions on the complexation with chitosan.: Application to the treatment of liquid waste. *European Polymer Journal*, 38(8):1523-1530, 2002.

87. Choi, J.-S., Yoon, S.-S., Jang, S.-H., and Ahn, W.-S. Phenol hydroxylation using Fe-MCM-41 catalysts. *Catalysis Today*, 111(3-4):280-287, 2006.

88. Ma, N., Ma, Z., Yue, Y., and Gao, Z. Reaction testing of phenol hydroxylation and cyclohexane oxidation by gas chromatography: Influence of residual hydrogen peroxide. *Journal of Molecular Catalysis A: Chemical*, 184(1-2):361-370, 2002.

89. Liang, X., Yang, R., Li, G., and Hu, C. Phenol hydroxylation over Fe-incorporated mesoporous materials prepared by coprecipitation. *Microporous and Mesoporous Materials*, 182:62-72, 2013.

90. Sharma, M., Saikia, G., Ahmed, K., Gogoi, S. R., Puranik, V. G., and Islam, N. S. Vanadium-based polyoxometalate complex as a new and efficient catalyst for phenol hydroxylation under mild conditions. *New Journal of Chemistry*, 42(7):5142-5152, 2018.

91. Bhagya, K. N. and Gayathri, V. Metal complexes of 2-methylimidazole encapsulated in zeolite-Y as efficient and reusable catalysts for oxidation of phenol and benzyl alcohol. *Journal of Porous Materials*, 20(1):257-266, 2013.

92. Yu, R., Xiao, F.-S., Wang, D., Sun, J., Liu, Y., Pang, G., Feng, S., Qiu, S., Xu, R., and Fang, C. Catalytic performance in phenol hydroxylation by hydrogen

peroxide over a catalyst of V–Zr–O complex. *Catalysis Today*, 51(1):39-46, 1999.

93. Jian, L., Chen, C., Lan, F., Deng, S., Xiao, W., and Zhang, N. Catalytic activity of unsaturated coordinated Cu-MOF to the hydroxylation of phenol. *Solid State Sciences*, 13(5):1127-1131, 2011.

94. Anjali, K., Ganesh, V., Christopher, J., and Sakthivel, A. Copper based macromolecular catalysts for the hydroxylation of phenols. *Journal of Organometallic Chemistry*, 929:121579, 2020.

95. Shringarpure, P. A. and Patel, A. Supported undecaphosphotungstate: An ecofriendly and efficient solid catalyst for nonsolvent liquid-phase aerobic epoxidation of alkenes. *Industrial & Engineering Chemistry Research*, 50(15):9069-9076, 2011.

96. Nandi, M. and Talukdar, A. K. Vanadia loaded hierarchical ZSM-5 zeolite: A promising catalyst for epoxidation of cyclohexene under solvent free condition. *Journal of Porous Materials*, 23:1143-1154, 2016.

97. Gogoi, S. R., Ahmed, K., Saikia, G., and Islam, N. S. Macromolecular metal complexes of Nb^V as recoverable catalysts for selective and eco-compatible oxidation of organic sulfides in water. *Journal of the Indian Chemical Society*, 95:801-812, 2018.

98. Gogoi, S. R., Boruah, J. J., Sengupta, G., Saikia, G., Ahmed, K., Bania, K. K., and Islam, N. S. Peroxoniobium(V)-catalyzed selective oxidation of sulfides with hydrogen peroxide in water: A sustainable approach. *Catalysis Science & Technology*, 5(1):595-610, 2015.

99. Conte, V. and Floris, B. Vanadium catalyzed oxidation with hydrogen peroxide. *Inorganica Chimica Acta*, 363(9):1935-1946, 2010.

100. Conte, V., Coletti, A., Floris, B., Licini, G., and Zonta, C. Mechanistic aspects of vanadium catalysed oxidations with peroxides. *Coordination Chemistry Reviews*, 255(19-20):2165-2177, 2011.

101. Trejda, M. and Ziolek, M. New iron containing mesoporous catalysts. *Catalysis Today*, 101(2):109-116, 2005.

102. Thornburg, N. E. and Notestein, J. M. Rate and selectivity control in thioether and alkene oxidation with H_2O_2 over phosphonate-modified niobium(V)–silica catalysts. *ChemCatChem*, 9(19):3714-3724, 2017.

103. Kirihara, M., Itou, A., Noguchi, T., and Yamamoto, J. Tantalum carbide or niobium carbide catalyzed oxidation of sulfides with hydrogen peroxide: Highly efficient and chemoselective syntheses of sulfoxides and sulfones. *Synlett*, 2010(10):1557-1561, 2010.

104. Sharpless, K., Townsend, J., and Williams, D. Mechanism of epoxidation of olefins by covalent peroxides of molybdenum(VI). *Journal of the American Chemical Society*, 94(1):295-296, 1972.

105. Yudanov, I. Mechanism of olefin epoxidation with transition metal peroxo complexes: DFT study. *Journal of Structural Chemistry*, 48(1):S111-S124, 2007.

106. Amini, M., Haghdoost, M. M., and Bagherzadeh, M. Oxido-peroxido molybdenum(VI) complexes in catalytic and stoichiometric oxidations. *Coordination Chemistry Reviews*, 257(7-8):1093-1121, 2013.

107. Kholdeeva, O. A., Ivanchikova, I. D., Maksimchuk, N. V., and Skobelev, I. Y. H_2O_2-based selective epoxidations: Nb-silicates versus Ti-silicates. *Catalysis Today*, 333:63-70, 2019.

108. Ruddy, D. A. and Tilley, T. D. Kinetics and mechanism of olefin epoxidation with aqueous H_2O_2 and a highly selective surface-modified TaSBA15 heterogeneous catalyst. *Journal of the American Chemical Society*, 130(33):11088-11096, 2008.

109. Chagas, P., Oliveira, H. S., Mambrini, R., Le Hyaric, M., de Almeida, M. V., and Oliveira, L. C. A novel hydrofobic niobium oxyhydroxide as catalyst: Selective cyclohexene oxidation to epoxide. *Applied Catalysis A- General*, 454:88-92, 2013.

110. Saikia, G., Ahmed, K., Rajkhowa, C., Sharma, M., Talukdar, H., and Islam, N. S. Polymer immobilized tantalum(v)–amino acid complexes as selective and recyclable heterogeneous catalysts for oxidation of olefins and sulfides with aqueous H_2O_2. *New Journal of Chemistry*, 43(44):17251-17266, 2019.

111. Boruah, J. J., Ahmed, K., Das, S., Gogoi, S. R., Saikia, G., Sharma, M., and Islam, N. S. Peroxomolybdate supported on water soluble polymers as efficient catalysts for green and selective sulfoxidation in aqueous medium. *Journal of Molecular Catalysis A: Chemical*, 425:21-30, 2016.

112. Das, S. P., Boruah, J. J., Sharma, N., and Islam, N. S. New polymer-immobilized peroxotungsten compound as an efficient catalyst for selective and mild oxidation

of sulfides by hydrogen peroxide. *Journal of Molecular Catalysis A: Chemical*, 356:36-45, 2012.

113. Ma, W., Yuan, H., Wang, H., Zhou, Q., Kong, K., Li, D., Yao, Y., and Hou, Z. Identifying catalytically active mononuclear peroxoniobate anion of ionic liquids in the epoxidation of olefins. *ACS Catalysis*, 8(5):4645-4659, 2018.

114. Ma, W., Qiao, Y., Theyssen, N., Zhou, Q., Li, D., Ding, B., Wang, D., and Hou, Z. A mononuclear tantalum catalyst with a peroxocarbonate ligand for olefin epoxidation in compressed CO_2. *Catalysis Science & Technology*, 9(7):1621-1630, 2019.